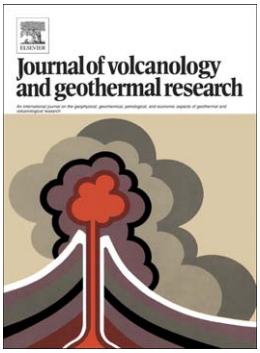

Volcanic hazard on Deception Island (South Shetland Islands, Antarctica)

S. Bartolini, A. Geyer, J. Martí, D. Pedrazzi, G. Aguirre-Díaz

PII: S0377-0273(14)00249-2
DOI: doi: 10.1016/j.jvolgeores.2014.08.009
Reference: VOLGEO 5385

To appear in: *Journal of Volcanology and Geothermal Research*

Received date: 22 May 2014
Accepted date: 8 August 2014

Please cite this article as: Bartolini, S., Geyer, A., Martí, J., Pedrazzi, D., Aguirre-Díaz, G., Volcanic hazard on Deception Island (South Shetland Islands, Antarctica), *Journal of Volcanology and Geothermal Research* (2014), doi: 10.1016/j.jvolgeores.2014.08.009

Volcanic hazard on Deception Island (South Shetland Islands, Antarctica)

S. Bartolini[a*], A. Geyer[a], J. Martí[a], D. Pedrazzi[a], G. Aguirre-Díaz[b]

[a] *Institute of Earth Sciences Jaume Almera, ICTJA-CSIC, Group of Volcanology, SIMGEO (UB-CSIC), Lluís Solé i Sabarís s/n, 08028 Barcelona, Spain.*

[b] *Centro de Geociencias, Universidad Nacional Autónoma de México, Campus Juriquilla, Querétaro, Qro. 76230, Mexico.*

[*] Corresponding author: tel.: +34 934095410; *E-mail address*: sbartolini@ictja.csic.es (S. Bartolini).

Abstract:

Deception Island is the most active volcano in the South Shetland Islands and has been the scene of more than twenty identified eruptions over the past two centuries. In this contribution we present the first comprehensive long-term volcanic hazard assessment for this volcanic island. The research is based on the use of probabilistic methods and statistical techniques to estimate volcanic susceptibility, eruption recurrence and the most likely future eruptive scenarios. We perform a statistical analysis of the time series of past eruptions and the spatial extent of their products, including lava flows, fallout, pyroclastic density currents and lahars. The Bayesian event tree statistical method HASSET is applied to calculate eruption recurrence, while the QVAST tool is used in an analysis of past activity to calculate the possibility that new vents will open (volcanic susceptibility). On the basis of these calculations, we identify a number of significant scenarios using the GIS-based VORIS 2.0.1 and

LAHARZ software and evaluate the potential extent of the main volcanic hazards to be expected on the island. This study represents a step forward in the evaluation of volcanic hazard on Deception Island and the results obtained are potentially useful for long-term emergency planning.

Keywords: Deception Island, volcanic hazard, volcanic susceptibility, Bayesian event tree, eruptive scenarios

1. Introduction

Deception Island is the most active volcano in the South Shetland Island group (Antarctica) and more than 20 eruptions have taken place there over the past two centuries (Orheim, 1972; Pallàs et al., 2001; Smellie, 2002a). Located at the spreading centre of the Bransfield Strait marginal basin (Fig. 1), this island consists of a horse-shoe-shaped composite volcanic system truncated by the formation of the collapse caldera that occupies the central part of the island (Valencio et al. 1979; Smellie 1988; Martí et al., 2013) (Fig. 2a). The most recent eruptions took place in the late 1960s and 1970s and destroyed or severely damaged the scientific bases operating on the island (Baker et al., 1975; Roobol, 1982) (Fig. 3a,b). Interestingly, during the final eruption strong winds and the unusually low tropopause in the area (Smellie, 1999) led to an important spread of volcanic ejecta that reached distances of over 150 km (Pallàs et al., 2001; Fretzdorff and Smellie, 2002; Pedrazzi et al., 2014).

Since its discovery in 1820, the island's natural harbours in Port Foster Bay (e.g. Pendulum Cove and Whalers Bay) (Fig. 2b) have been actively used during different peaks in the commercial exploitation of the Southern Ocean (Roobol, 1982; Smellie and López-Martínez, 2002). Between 1905 and 1930, the island served as the shore base for the Antarctic's most important whaling industry (Fig. 3c) and also played a military role during World War I due to its strategic location between the Atlantic and Pacific Oceans. This resulted in the construction of a British scientific station, which was occupied from 1944 until it was destroyed in 1969 (Roobol, 1982; Smellie and López-Martínez, 2002) (Fig. 3a). Following the British initiative, Argentina and Chile also established scientific bases on the island that, likewise, were either destroyed or abandoned after the eruptions occurring between 1967 and 1970 (Fig. 3b). After occasional expeditions to Deception Island, Britain, Spain and Argentina recommenced scientific activity in 1986. Argentina

re-occupied and reconstructed its station (Fig. 3f), while Spain constructed a new station in 1989 (Fig. 3e); these two scientific bases operate every year during the Antarctic summer.

The number of tourists that visit Antarctica has increased since the first commercial cruise in 1966 and today over 30,000 visitors arrive during the austral summer (2012-2013) (IAATO, *International Association of Antarctica Tour Operators*) (Fig. 4a). Deception Island and Half Moon Island (Fig. 4) are two of the most popular destinations; specifically, the Antarctic Specially Protected Area (ASPA) sub-site of Whalers Bay (Fig. 2) receives over 15,000 visitors every year (Fig. 4b), while other sectors such as Telefon Bay or Pendulum Cove (Fig. 2) are visited by up to 5,000 tourists annually (Fig. 4b).

The recent eruptions (1967, 1969 and 1970) have demonstrated that volcanic activity on Deception Island may become a cause for concern for tourists, scientists and the military personnel working on or near the island. Livingston and Deception Islands host a total of five research stations and three field camps, while Greenwich and King George Islands are home to 10 all-year and two temporary research stations (Fig. 2). For example, during the 1970 eruption, a considerable amount of ash – including a fine ash fall deposit of 4 mm on Arturo Prat station on Greenwich Island and about 1 mm on Bellingshausen station on King George Island (Baker et al., 1975, Pedrazzi et al., 2014) – fell far from the island.

Aside from a paper by Roobol (1982) and the relatively recent work of Smellie (2002a), to the authors' knowledge no accurate volcanic hazard assessment has ever been conducted for Deception Island. Furthermore, previously hazard maps were either restricted to a single hazard (Roobol, 1982) (Fig. 5a) or were non-systematic (Smellie, 2002a) (Fig. 5b). As pointed out by Smellie (2002a), as a popular destination for tourists

and an area of constant scientific research, properly elaborated hazard maps and related assessments are now more necessary than ever. The latter are indispensable for the elaboration of emergency plans aimed at mitigating the potential human and economic losses of any future volcanic eruptions on Deception Island.

In order to improve the hazard assessment on Deception Island, it is important to estimate the temporal and spatial probabilities of future eruptions. In this paper, we carry out a threat analysis for Deception Island using the National Volcano Early Warning System (NVEWS) template (Ewert et al., 2005) and compare it with other volcanoes of similar characteristics. Then, we present a systematic analysis of the temporal and spatial long-term hazard assessment of the island using available geological data, including the past eruption record, stratigraphic information and volcano-structural data. We used HASSET (Sobradelo et al., 2014) to estimate the probability that a volcanic episode will occur within the forecast interval and to evaluate the long-term probability of different types of hazards on the island. For the spatial analysis we applied QVAST (Bartolini et al., 2013) to obtain the susceptibility map, and LAHARZ and VORIS (Hoblitt et al., 1995; Schilling, 1998; Felpeto et al., 2007) to generate different eruptive scenarios such as lahars, lava flows, pyroclastic density currents (PDCs) and fallout. The ultimate aim of this work was to generate a qualitative hazard map for Deception Island depicting the most probable scenarios and, consequently, to understand the potential impact that future eruptions could have on research stations, tourists, and ships in and around the island.

2. Geological setting

Deception Island is a sizeable active Quaternary volcano with a large central

collapse caldera that is located at the south-western end of the Bransfield Strait, a marginal basin lying between the Antarctic Peninsula and the South Shetland Islands (Fig. 1). The related volcanic ridge has traditionally been interpreted as a Late Cenozoic extensional structure produced as a consequence of back-arc spreading (Roach, 1978; Peccerillo et al., 1991) linked to subduction of the Phoenix Plate beneath the Antarctic Plate (González-Ferrán, 1985). Deception, Penguin and Bridgeman islands and a number of other submerged volcanic vents are associated with the spreading centre. In particular, Deception Island is located near the intersection between the axis of the Bransfield basin and the extension of the Hero Fracture Zone (Fig. 1).

The construction of the island can be separated into three main phases: pre-, syn- and post-caldera (Smellie, 2001; Martí et al., 2013). The first phase was characterised by the construction of the volcanic shield and is represented by the Basaltic Shield Formation, outcropping mainly at Baily Head and along the nearly vertical caldera wall at Fumarole Bay (Fig. 2a). The Outer Coast Tuff Formation (i.e. syn-caldera phase deposits) (Hawkes, 1961; Smellie, 2001; Martí et al., 2013) was deposited unconformably over the shield-related units and forms an almost continuous outcrop along the outer part of the island (Fig. 2a). The post-caldera phase, which includes the recent historical eruptions, consists of eruptive vents scattered across the whole island: all but one are found along the structural borders of the caldera and most correspond to previous regional tectonic faults (Fig. 2a) (Smellie, 2002a; Martí et al., 2013).

The magnetic polarity of the exposed rocks and K-Ar data indicate that Deception Island is younger than 0.75 Ma (Valencio et al., 1979) and that its subaerial part has mostly been constructed over the last 0.2 Ma (Keller et al., 1992). Indeed, the correlation between the exposed rocks and the tephras found elsewhere in the region suggests that these rocks are probably even younger than 0.1 Ma (Martí et al., 2013).

The age of the collapse event remains unclear due to a lack of geochronological data and the fact that none of the tephra layers found in the various ice and marine/lacustrine sediment cores extracted around the Antarctic region appear to correlate with this event (Smellie, 1999; Pallàs et al., 2001). Since all the tephra related to the post-caldera volcanism recorded in the region are from the Middle Holocene or younger (Smellie, 1999; Moreton, 1999), Martí et al (2013) speculate that the caldera may have formed in the late Pleistocene-early Holocene.

3. Recent Volcanic Activity & Volcanic Hazards

The 1967, 1969 and 1970 eruptions on Deception Island have been well documented (González-Ferrán et al., 1971; Orheim, 1972; Baker et al., 1975; Roobol, 1982; Smellie, 1999, 2002a, 2002b; Moreton, 1999; Pedrazzi et al., 2014). First-hand observations exist for the first two as they occurred during austral summer. The December 1967 event created a new island around four aligned vents in Telefon Bay and a land vent located 2.5 km to the east (Fig. 2b). The February 1969 eruption occurred when a 4-km-long fissure opened beneath glacial ice along the eastern interior side of the caldera (Smellie, 2002a). This activity resulted in catastrophic floods and lahars, and the construction of several small cinder cones (Baker et al., 1975; Smellie, 2002b). Unlike the two previous events, there were no eyewitnesses to the 1970 eruption. Ash fell on the Chilean station *Arturo Prat* on Greenwich Island on August 13, 1970 and during the early morning on the same day near the Soviet station *Bellingshausen* on the King George Islands.

The tephra record from Deception Island (Orheim, 1972) and neighbouring islands (Pallàs et al., 2001) and ice and sediment (marine and lacustrine) cores reveal a series of over 30 post-caldera eruptions during the Holocene (Tables 1 and 2). However, even the most detailed record such as that provided by Mt. Pond glacier (Fig. 2a) probably only records some of the post-caldera eruptions on the island (Orheim, 1972; Smellie, 2002b) and a considerably higher number of eruptions may well have occurred. The record of the eruptions from the eighteenth to the twentieth centuries includes periods of great activity (e.g. 1906–1912, 1818–1828) with several temporally closely spaced eruptions, followed by decades of dormancy (e.g. 1912–1967) (Orheim, 1972; Roobol, 1982; Smellie, 2002b). Despite the inherent difficulties involved in predicting the date of the next eruption on Deception Island, it is still reasonable to expect further episodes to occur as part of these most recent activity cycles (Shultz, 1972). The unrest episodes in 1992 and 1999 demonstrate that the volcanic system is still active (Ibañez et al., 2003) and, as has been remarked in published research work, the occurrence of a future eruption on the island cannot be ruled out.

All post-caldera volcanism corresponds to eruptions of small volume (e.g. < 0.05 km^3 for each of the 1967, 1969, and 1970 eruptions) and their explosivity will have varied in terms of their consistent phreatomagmatic nature. The interacting water may be simply seawater from Port Foster Bay, water from the underground aquifer or even melt water from the glaciers. The presence of Deception Island tephra in marine sediments in the Scotia Sea (e.g. Moreton and Smellie, 1998) or in ice cores from the South Pole (e.g. Aristarain and Delmas, 1998) suggests that some post-caldera eruptions may have been much more violent than those experienced in recent centuries.

The main direct volcanic hazards identified on Deception Island include (Smellie, 2002a) ash fall, pyroclastic density currents (mainly surges), lava flows and

lahars, while indirect volcanic hazards could involve (Smellie, 2002a) steam fields, fumaroles, heated ground, structural collapses and rock falls, hydrothermal eruptions, volcanic gases, earthquakes and tsunamis.

Due to the strong winds and the unusually low tropopause (8-10 km) in the area (Smellie, 1999), ash fall deposits – even in historical eruptions – are rapidly displaced over neighbouring islands and the Antarctic continent. Indeed, ashes from the latest eruption on Deception Island were observed on King George Island (>150 km distance) (Baker et al., 1975). Additionally, numerous layers of Deception Island ash are preserved in marine sediments in the Scotia Sea (>800 km distance) (Moreton and Smellie, 1998). Close to the vent, ash fallout can lead to severe building damage, as in the case of the abandoned Chilean station at Pendulum Cove (Fig. 3b). This base was covered (and burned down) by ash from the 1969 fissure eruption, the closest vents of which were 400–500 m away (Smellie, 2002b). Smellie (2002a) has pointed out that since the prevailing winds on Deception Island are mainly from the west, the eastern side of the island is highly exposed to ash fall. Nevertheless, during the most recent eruptions, almost the entire island received some ash fall (Baker et al., 1975; Smellie, 2002a).

In the first volcanic hazard assessment on Deception Island, Roobol (1982) indicated that there were no relevant pyroclastic flows on the island. Nevertheless, Smellie (2002a) specifies that pyroclastic flows have occurred in the past but were only abundant during the caldera-forming eruption (Outer Coast Tuff Formation). Even so, dilute pyroclastic density currents (i.e. pyroclastic surges) are a characteristic feature of many Deception Island post-caldera eruptions. In most cases, mapped surge deposits extend for about 2 km from the vents (Pedrazzi et al., 2014) and may travel across water (Smellie, 2002a).

Lava fountaining and flows have also been a common feature throughout the eruptive history of the island (Roobol, 1982; Smellie, 2002a). The main hazard related to lava flows is the damage or destruction they cause by burying, crushing or burning as they progress. Even though they tend to be confined to valleys and can be easily outrun, the most important problem is that they can generate *jökulhlaups*, i.e. floods of molten water released from the glacier due to the opening of subglacial vents and the partial melting of the ice cover (Roobol, 1982; Smellie, 2002a, 2002b). In fact, Baker et al. (1975) state that the most recent eruptions demonstrate that these floods are the main hazards to human life and property on the island. The same authors indicate that the most suitable sites for scientific stations on the shores around Port Foster are also the most vulnerable to the effects of this particular hazard.

These lahars or volcanic mudflows consist of substantial volumes of melt water, often highly charged with debris. Their great bulk density and velocity make them highly destructive. In fact, the *jökulhlaups* produced by the 1969 eruption were responsible for the destruction of the British scientific station at Whalers Bay (Baker et al., 1975). Lahars are characterised by having well-defined topographical limits since they are confined to valleys (Smellie, 2002a). Thus, the location of the eruptive vent, i.e. in ice-free areas or below the permanent ice caps on Mt. Kirkwood and Mt. Pond (Fig. 2b), is crucial for determining the potential hazards to be expected during a future eruption on Deception Island.

Other secondary hazards such as steam fields, fumaroles and ground heating are also common on the island, and are mostly confined to the inside of the caldera along the shores of Port Foster (Baker et al., 1975; Roobol, 1980; Smellie, 2002a) (Fig. 2b). Ground temperatures of <40-60ºC are common but at Pendulum Cove and Fumarole Bay, they may reach up to 70ºC and 100ºC, respectively (Smellie, 2002a). These

temperatures fluctuate daily, mainly with the tides. In 1920–21, for example, sudden subsidence of the sea floor beneath Whalers Bay caused the sea to boil and affected the ships in the area (Smellie, 2002a).

Seismicity may also be an issue in the area. During 1992 and 1999, two seismic crises related to episodes of deep magma injection led to the evacuation of the island (Ibañez et al., 2003). In general terms, current activity is characterised by strong hydrothermal circulation and intense seismicity with frequent volcano-tectonic and long-period events (Smellie, 2002a; Zandomeneghi et al., 2009).

In addition, tsunamis triggered by eruptions and slope failures have occurred on Deception Island in the past (Smellie, 2002a). This is an important problem since they may block Neptune's Bellows, the only exit from (and entry into) Port Foster and make it difficult or even impossible to sail through this narrow, shallow channel. On a smaller scale, rock falls in strategically important places could cause major problems and, for example, the collapse of Cathedral Crags could block Neptune's Bellows and prevent ships from entering/leaving the island's interior bay (Smellie, 2002a).

4. Threat Analysis

The quantification of the threat posed by volcanoes to their surroundings is vital when trying to define the required monitoring level for each volcano. In order to perform this quantification, Ewert et al. (2005) developed the National Volcano Early Warning System (NVEWS). The rationale behind NVEWS was to assess the threat posed by volcanoes in the United States via an analysis scheme divided into two main factor groups. First, those directly associated with the volcanic hazard and second, those related to exposure of human, social and economical elements potentially affected by the hazard. The individual factors are summed into a hazard score and an exposure

score, which are then multiplied to generate the volcano's overall threat score. The total threat score obtained classifies the volcanic threat into one of five threat categories (Ewert et al., 2005): very low (6-0), low (6-30), moderate high (30-63), high (63 -113) and very high (> 113).

In recent years several authors have applied the NVEWS analysis to other volcanoes (e.g. Kinvig et al., 2010; Martí et al., 2012). Scores given to each factor (labelled from (a) to (y)) and the final results are given in Table 3. A brief explanation of the different scores is included in the next section; full details and references for the NVEWS analysis performed for Deception Island is included as a Microsoft Excel spread sheet in Supplementary Material 1. For each factor we have tried to determine the maximum and minimum score in an attempt to quantify the uncertainty caused by the lack of data in some cases. The obtained threat score for Deception Island is between 107.2 and 180, which corresponds to a high-to-very-high level of threat (Ewert et al., 2005).

4.1. Hazard factors

Deception Island corresponds to a composite volcanic system that includes a central collapse caldera that was responsible for the creation of Port Foster (a). Nevertheless, post-caldera volcanism is apparently restricted to small-size eruptions up to VEI 4, as indicated by the deposits on the island and the tephra records elsewhere in the region (b). Some indices of bimodal volcanism and deposits found at distances of over 500 km away suggest that more powerful eruptions may have taken place (e.g. Aristarain and Delmas, 1998; Caselli and Agusto, 2004; Smellie, 2002a) (c) and (d).

The historical period in Deception Island is relatively short as it starts in 1820. Since then, over 15 eruptions have occurred on the island at Mt. Kirkwood (e.g. 1842,

1838–1839), Mt. Pond (e.g. 1969), Whalers Bay (e.g. 1829–1908), Pendulum Cove (e.g. 1800–1828, 1830–1927, 1931–1955) and Telefon Bay (e.g. 1967, 1970). During the Holocene, at least 30 eruptions occurred on Deception Island (Tables 1 and 2) including all the volcanic hazards described in the previous section (e). As mentioned above, there is evidence of pyroclastic surges and flows (f), lava flows (g) and ash fall. The constant fumarolic activity on the island and the evidence of phreatomagmatic eruptions fully justify the hydrothermal potential of the island (Smellie, 2002a) (h). There is also evidence of sector collapses (k) that may have led to tsunamis (j) inside Port Foster or beyond the island (Smellie, 2002a). As well, the permanent ice on Mt. Pond and Mt. Kirkwood also provide a primary source for a lahar in the event of an eruption occurring underneath these ice caps (l).

In 1992 and 1999, an episode of volcanic unrest took place on Deception Island that was characterised by a great increase in seismic activity (m) and changes in the hydrothermal system and fumarolic activity (o) (Ibañez et al., 2003). Ground deformation has been also observed on the island during recent scientific surveys (e.g. Prates et al., 2013) (n).

4.2. Exposure factor

When evaluating the threat on Deception Island it is important to take into account the fact that it is only populated during the austral summer. However, in neighbouring areas a few stations are inhabited during the winter and there is a permanent population on King George Island (Fig. 1). Thus, the threat analysis presented here refers mainly to the summer, especially for the maximum scores.

The first exposure factor is the volcano population index (VPI) within a 30-km radius of the volcano summit or the most recent active event. On Deception Island, this

distance consists of the entire island and includes the Spanish and Bulgarian bases on Livingston Island (Fig. 1). These two bases, together with the ones on Deception Island itself, may be home to 50–100 people (i.e. a VPI of 1.7–2) (p). However, as one of the main Antarctic touristic destinations, we should also consider the possibility that a fully laden tourist vessel is present on the island, with which the VPI increases to 3 or more. There is no population downstream of the volcano within the 30 km VPI circle (q) and no fatalities have ever been recorded during the eruptions on Deception Island (r). The Chilean and British stations and the Argentinian and Spanish bases were evacuated during the 1967 and 1969 eruptions and the seismic crisis of 1992, respectively (Ibañez et al., 2003, Smith et al., 2003), and no permanent populations remain (s).

In terms of local aviation exposure, the only airport on the South Shetland Islands is on King George Island, about 150 km away (t): a maximum of two flights per day would represent around 100 passengers (u). The power infrastructures for both the Spanish and the Argentinian bases and all accessible ports within Port Foster (e.g. Whaler's Bay or Pendulum Cove) are located within the flowage hazard zones (v), (w). Finally, several parts of the island are considered Antarctic Specially Protected Areas and the Holocene volcanic deposits cover over 25% of the island landmass (x), (y).

5. Volcanic hazard assessment: spatial and temporal analysis

The main steps in the volcanic hazard assessment on Deception Island (Fig. 6) can be divided into long- and short-term analyses. Long-term hazard assessment is based on the past history of the volcano and requires information from the geological record. This analysis enables us to determine the eruption recurrence and the possible nature of a forthcoming eruption. Short-term hazard assessment, on the other hand, provides complementary information resulting from the combination of a long-term

analysis with real-time monitoring data gathered during a crisis or an unrest episode, and helps forecast where and when the eruption might take place and the most likely eruptive scenarios. To evaluate the long-term volcanic hazard, for this study we carried out both temporal and spatial analyses: the former evaluates in a probabilistic way possible outcomes of volcanic unrest within a specific time frame, while the latter uses simulation models to predict the most probable eruptive scenarios and which areas could be affected by a future eruptive event. The susceptibility analysis enables us to identify which areas have the greatest likelihood of hosting new vents.

Since the results from these temporal and spatial analyses are highly dependent on the data used, the selection of the data source is one of the most important steps to be undertaken during a hazard evaluation. Due to the logistic difficulties involved in performing repeated field studies or other surveying in the area, only previously published peer-reviewed information has been used in addition to our own data in this systematic volcanic hazard assessment. In the coming sections we provide a general overview of the different tools applied in this study, as well as a careful description of the required input data. For further detailed information regarding each specific tool, readers are referred to the original papers.

5.1. Susceptibility analysis

The first step in a long-term spatial analysis is to evaluate the susceptibility (probability of vent opening; Martí and Felpeto, 2010) of the volcanic area. For Deception Island we paid special attention to recent volcanic structural indicators such as vent locations and alignments, fumarolic activity and heated ground sites (Fig. 2). Vent locations were divided into post-caldera craters (no precise dating but recognisable in the field and from satellite images) and the historical volcanism described in the

bibliography (Wilkes, 1845; Valenzuela et al., 1970; González-Ferrán et al., 1971; Baker et al., 1975; Roobol, 1980; Smellie, 2002b; Pedrazzi et al., 2014). The lineament structures shown in Figure 2a are taken from the simplified structural map of Deception Island in Martí et al. (2013). On the island, a NE–SW oriented regional tectonic trend, almost parallel to the expansion axis of the Bransfield Strait, is clearly predominant; NW–SE and N–S oriented faults are also present (Martí et al., 2013). Figure 2b also includes those areas with clear signals of hydrotermal processes such as fumaroles or heated ground that can be related to the heating of shallow aquifers by convection gaseous inflowing from the underlying magma intrusions (Ortiz et al. 1987; Ramos et al. 1989; Rey et al., 1995; López-Martínez et al., 2000; Patrick and Smellie, 2013).

Susceptibility is generally calculated using probabilistic methods that estimate probability density functions (PDFs) by calculating a kernel function for each data location (Martin et al., 2004; Felpeto et al., 2007; Connor et al., 2012; Cappello et al., 2012, 2013; Becerril et al., 2013; Bartolini et al., 2013). The smoothness and the modelling ability of the kernel function is controlled by the smoothing parameter or bandwidth *h*, which determines how the probabilities spread out from the volcanic structures or vents (Diggle, 1985; Connor and Hill, 1995; Lutz and Gutmann, 1995; Cappello et al., 2012). Thus, for small *h* values, the kernel function gives high probability estimates in the vicinity of the existing volcanic structures. Conversely, when high bandwidth values are assigned, the probability estimates are distributed in a more homogeneous way throughout the entire area under study. The *h* values obtained for our dataset from Deception Island are given in Table 4.

For the present work, the bandwidth and the corresponding Gaussian Kernels and PDFs for all available datasets (vent locations, vent alignments, dykes, etc.) were evaluated with QVAST (Bartolini et al., 2013). We chose the modified version of the

Least Square Cross Validation (LSCV) method to evaluate *h* (Cappello et al., 2012, 2013) and computed the final susceptibility map (Fig. 7) assuming a non-homogeneous Poisson process. To obtain the final susceptibility map, we had to combine all the PDFs evaluated for each volcano-structural data in a weighted sum. These weights were assigned using expert elicitation judgment (see Aspinall, 2006; Neri et al., 2008) by experts from the Group of Volcanology of Barcelona on the basis of structural criteria (see Martí and Felpeto, 2010), which provide initial indicative probability distributions associated with each PDF. We obtained the following values: 0.4 for the historical volcanism, 0.4 for the post-caldera craters, 0.1 for lineament structures, 0.05 for fumarolic activity and 0.05 for heated ground.

5.2. Temporal analysis

The temporal analysis was computed using HASSET (Sobradelo et al., 2014), an event tree structure that uses Bayesian inference to estimate the probability of occurrence of a future volcanic scenario (Sobradelo and Martí, 2010) and to predict the five most likely scenarios. An event tree is a probabilistic model that can be used to calculate the probability of occurrence for any possible volcano-related event (Newhall and Hoblitt, 2002; Aspinall and Woo, 1994; Marzocchi et al., 2008, 2010; Aspinall, 2006; Neri et al., 2008; Martí et al., 2008; Sobradelo and Martí, 2010; Becerril et al., 2014). This graphic representation of events in the form of nodes and branches depicts all relevant possible outcomes of volcanic unrest in progressively greater levels of detail.

Input data for the HASSET event tree model consists of geological and/or physical models, past data, present and past monitoring observations, and expert opinion. Three parameters must be entered at each branch to run the model: past data,

prior weight and data weight (Sobradelo and Martí, 2010; Sobradelo et al., 2014). Past data consists of information about the volcanic area corresponding to observational data or data collated from the bibliography. We assume that the future behaviour of the volcano will be similar to its recent past history. In probabilistic terms, prior weight represents uncertainty before data are gathered and it is assigned on the basis of the *priori* beliefs regarding the volcanic area under study. Data weight represents how well we know the system. This value represents the epistemic uncertainty related to our knowledge of the system and the quality and quantity of data we have about the system. The more data we have, the better we know the system and the lower the epistemic uncertainty (Woo, 1999; Sobradelo and Martí, 2010).

The study of temporal probability on Deception Island was based on the catalogue of eruptions documented in Tables 1 and 2. Information from these eruptions was used to characterise past eruptive activity and to estimate some of the input parameters required for our hazard assessment. Due to the certainty that not all post-caldera eruptions occurred on Deception Island have been identified and/or dated, we computed only those volcanic eruptions and unrest periods recorded for the last 372 years (1641–2013), the period for which the available stratigraphic record and geochronological data are most precise. Therefore, using HASSET we were able to estimate the probability of a volcanic episode occurring within the forecasting time interval (the following 2 years). This forecasting time interval was chosen on the basis of the model and represents the minimum time window range needed to evaluate the probability of having at least one eruption in the range considered (see Sobradelo and Martí, 2010). The time window of the dataset is 372 years and so we obtained 186 time intervals of data for the study period. As we restricted our dataset to the last 372 years, the eruptions in this catalogue were used to assign prior weights to nodes 2 to 8. Table 5

shows the Bayesian event tree structure for Deception Island, as well as the input parameters for each branch. Figure 8 shows the probability for each event tree branch.

Furthermore, using HASSET it is possible to compute the total probability for any particular scenario and then compare results. Once all probability density functions for each branch of each node and the conditional probability assessment are calculated, all these probabilities can be combined to estimate the total long-term probability of a particular event. Thus, we evaluated the total probability for different eruptive scenarios for the five different sectors that we established for Deception Island according to susceptibility and topographic criteria, as is permitted by HASSET and explained below (Fig. 9).

Node 1: Unrest

This first node estimates the temporal probability that the system will reactivate during the next time window. The probability that an unrest phase will occur (or not) during the next time window can be obtained by analysing the number of past time windows that encompass an episode of unrest. It does not take into account the periods of repose between eruptions or the possible non-stationary nature of the data (Sobradelo and Martí, 2010; Sobradelo et al., 2014).

As mentioned above, the existing eruptive record of Deception Island may be incomplete. First, the island is uninhabited for most of the year and so direct observations of unrest periods, whether a prelude or not to a volcanic eruption, are clearly biased towards the period when observers are present. Second, most of the information comes from ice-core studies and reports from Antarctic expeditions. Thus, the number of unrest periods occurring during the temporal window used in this analysis may be underestimated. For this reason, we assigned an epistemic uncertainty

of 10 to our data weights, which means that new evidence on intervals with eruptive or non-eruptive behaviour will modify our prior assumptions. We assigned a 0.30 *prior* weight to unrest and 0.70 of prior weight to 'no' unrest.

Node 2: Origin

The origin node takes into account four types of unrest that could occur in a volcanic area: magmatic involving the movement of fresh magma, geothermal, seismic and others. Two intense seismic crises in 1992 and 1999 have been registered in 15 years of monitoring (Ibañez et al., 2003). This high seismicity was probably associated with the activity of the main geothermal system installed inside the caldera depression (Martí et al., 2013). Despite the predominantly magmatic character of past activity on the island, we cannot exclude the possibility of geothermal behaviour without any associated fresh magma movements as occurs in other caldera systems with high geothermal activity (e.g. Campi Flegrei, Gottsmann et al., 2006; Nysiros, Gottsmann et al., 2007). In this sense, we have to assume that seismo-volcanic signals can also be associated with a shallow geothermal aquifer and deep hot materials (but not necessarily fresh magma), which gives rise to the resonance of fluid-filled fractures (Ibañez et al., 2003). In fact, these seismic measurements are not continuous and have only been registered over the past 15 years; there is thus a lack of seismic information and other similar but unrecorded periods of intense seismic activity may have gone unnoticed (Ibañez et al., 2003). For this reason, we assigned 0.5 for magmatic origin, 0.4 for geothermal origin, and split the rest evenly among the other options.

The prior weights are assigned on the basis of *a priori* beliefs and so we assigned a value of 10 to the epistemic uncertainty since we still expect the majority of

unrest to be of magmatic origin. However, it is important to give a certain weight to new evidence.

Node 3: Outcome

A study of volcanic unrest in the historical period of Deception Island shows that 84% of unrest episodes have led to eruptions. Only three documented unrest periods failed to generate volcanic activity. The lack of information about seismic activity caused by hydrothermal behaviour suggests that many other episodes of 'no eruption' could have occurred in addition to the documented ones. For this reason, we assigned 0.60 to magmatic eruption and 0.30 to 'no eruption'. The remaining 0.10 was split into the possibility of a phreatic explosion (prior weight of 0.8) and a sector failure (prior weight of 0.2) following an episode of unrest.

Given that these weights were assigned on the basis of incomplete data, we assigned a value of 10 to the epistemic uncertainty. We did not assign total epistemic uncertainty as we still believe that the largest weight should be for the magmatic eruption with no eruption branches; however, we still want new evidence to be able to contribute significantly to the updating of our prior weights.

Node 4: Location

The location node divides Deception Island into five main zones according to its topographic characteristics and the nature of past activity (volcanic susceptibility and past hazards). The five zones are shown in Figure 9.

Mount Pond (zone 1) and Mount Kirkwood (zone 4) represent zones with the presence of extensive glaciers on their summits. The 1969 subglacial eruption took place on Mount Pond (Smellie, 2002b) and gave rise to the Costa Recta, a retreated

scarp produced by a normal NNW–SSE-orientated fault (Fernández-Ibañez et al., 2005). Mount Kirkwood is characterised by the lava flows from the 1842 eruption. In the vicinity of Mount Kirkwood there are two scientific-military bases, the *Deception* base (Argentina) and the *Gabriel de Castilla* station (Spain), both of which only operate during the Antarctic summer. The eruptive episodes from 1967 and 1970 were located on Telefon Ridge (zone 2) and Telefon Bay was largely filled by products from these eruptions, although three new smaller bays were created in flooded craters that formed during the final eruption in 1970 (Smellie, 2001). Stonethrow Ridge (zone 3) was formed after the caldera collapse and is characterised by lava flows and deposits of red and black scorias (Augusto et al., 2007). Port Foster (zone 5), the sea-flooded depression formed by the caldera collapse, occupies the central part of the island and is characterised by major normal faults bounding the caldera depression (Maestro et al., 2007; Martí et al., 2013).

The susceptibility analysis of the island based on the methodology described above allows us to assign prior weights to each node with a high degree of confidence, as shown in Table 5. The reliability of the susceptibility map allows us to assign a data weight of 50 since the prior weights were estimated using past data from Deception Island based on the volcano-structural data and on the location of past and current hydrothermal activity. For this reason, we are confident of the initial distribution of these prior weights.

Node 5: Composition

Most of the post-caldera volcanic activity on Deception Island corresponds to the eruption of basaltic and andesitic magmas (González-Ferrán et al., 1971; Smellie, 2001), of which only one is of dacitic composition (Table 1). Therefore, we assigned a

wait of 0.95 for mafic composition and 0.05 for felsic composition. We assigned an epistemic uncertainty of 50, which means that new evidence regarding the composition of the historical eruptions will not modify substantially our prior assumptions.

Node 6: Size

The erupted volume on Deception Island ranges from 0.01 to 0.1 km^3 of magma, with post-caldera activity varying from magmatic Strombolian to phreatomagmatic sub-Plinian in nature (Baker et al., 1975; Keller et al., 1992; Smellie, 1988, 1999). The values that characterize this activity on the island can be linked to small batches of deep-sourced magmas (Martí et al., 2013). Taking into account the recorded data, we attributed to VEI<= 2, VEI =3 and VEI >=4, the values of 0.10, 0.70 and 0.20, respectively. We assigned as a prior weight for the epistemic uncertainty a value of 10 as new evidence on the volumes or sizes of the historical eruptions will help significantly update our prior knowledge.

Node 7: Hazard

Post-caldera eruptions are characterised by the generation of ballistic ejecta, scoria fallout, PDCs, lava flows and lahars. Based on information on past activity, we assigned 0.3 for both ballistic ejecta and fallout, 0.2 for PDC, 0.12 for lava flows, 0.03 for both lahars and debris avalanches, and 0.02 for others. However, for the same reasons given for the size weights, we assigned a value of 30 to the epistemic uncertainties, as these prior weights may vary somewhat if an improved data catalogue – especially based on studies of the ice record – of past volcanic deposits can be obtained.

Node 8: Extent

Node extent refers to the distance reached by eruption products such as lava flows, ballistic, fallout, lahars and PDCs. The extent of the recent volcanic products on Deception Island varies considerably and, while lava flows may emplace only very close to the vents, ash fallout can be carried over 100 km due to the strong winds and the characteristic tropopause height of the area. In this analysis, we considered products located near the vents to be of small extent, products emplaced on the island to be of medium extent, and products emplaced beyond Deception Island to be of large extent. According to this and the geological record, 0.1 of extents were small, while 0.3 were medium and 0.6 large. We assigned an epistemic value of 50 to all branches, as new data will not affect significantly this information.

5.3. Eruptive scenarios

The second step is to simulate different eruptive scenarios using information on the spatial probability of a new vent opening indicated on the calculated susceptibility map. The result is a final qualitative hazard map created by the superposition of the different analysed scenarios. Simulations were conducted using VORIS 2.0.1 (Felpeto et al., 2007; available at http://www.gvb-csic.es/GVB/VORIS/VORIS.htm) and LAHARZ (Schilling, 1998; available at http://vulcan.wr.usgs.gov/Projects/LAHARZ/framework.html), two automatic systems developed in a GIS framework (ArcGis®) that enable volcanic hazard maps and eruptive scenarios based on geological record information to be elaborated. The VORIS 2.0.1 tool generates quantitative hazard maps for lava flows and PDCs and simulates fallout deposits for a single vent. LAHARZ is able to map lahar inundation zones.

Eruptive scenarios were calculated using information from recent historical

eruptions and on the basis of the premise that future eruptions (if any) will be similar to those documented on the island from 1842, 1967, 1969 and 1970. Taking into account the main types of primary volcanic hazards identified during the historical eruptions (Smellie, 2002a), the eruptive scenarios predict the existence of ash fall, lava flows, dilute pyroclastic density currents and lahars. Furthermore, as obtained in the Bayesian Event Tree analysis, we have also a not null probability for ballistic ejecta and debris avalanches hazards. In this first analysis, we have decided not to include these two hazards due to the scarcity of input parameters to run the models.

5.3.1. Ash fall

Ash fall can be expected to occur on Deception Island in the event of more than one type of eruptive style. The style considered in this study was a violent Strombolian eruption, which coincides with recent eruption styles and corresponds to the most significant hazard in terms of probability of occurrence according to the long-term event tree constructed in section 5.2. Temporal probability. The input data regarding the eruptive column and ash particle size were inferred from the 1967, 1969 and 1970 eruptions (Valenzuela et al., 1970; González-Ferrán et al., 1971; Baker et al., 1975; Roobol, 1980; Smellie, 2002b; Pedrazzi et al., 2014), which were relatively small in volume (<0.05 km^3) with eruptive columns that were probably less than 10-km high (Smellie, 2002b; Pedrazzi et al., 2014). Ash fallout simulations were based on the advection-diffusion model (Folch and Felpeto, 2005), whereby the vertical mass distribution is computed using Suzuki's approximation (Suzuki, 1983; Felpeto et al., 2007). Wind data for the advection model correspond to records from the *Bellingshausen* station and were provided by the British Antarctic Survey (http://www.antarctica.ac.uk/met/READER/upper_air/uawind.html). Monthly records

were used to calculate average annual wind velocities and directions at intervals of about 1,500 m up to an altitude of 20,000 m for a 30-year period (from 1969 to 1999). The wind roses for the time period considered are included as Supplementary Material 2.

We focused our attention on the fallout scenarios corresponding to the average wind velocity and direction values for each season. Up to five different wind direction inputs and intensities at different vertical heights can be used with the VORIS 2.0.1 tool. We chose data from altitudes between 1,500 and 12,000 m. Westerly winds prevail in general throughout the year, but with a more north-westerly direction in summer and winter. This is due to the fact that the data used come from a station that is strongly affected by the climatological low pressure that forms over the Bellingshausen Sea that generates predominantly north to north-westerly winds (Turner and Pendlebury, 2004). Wind speed averages range between 20 and 50 m/s. All the simulations were conducted assuming a single eruptive vent located in the area with the highest spatial probability during each season.

Results are shown in Figure 10, with particles distributed in a 5-km-high eruptive column produced by a violent Strombolian eruption generating 0.03 km^3 of deposits. The column height and volume values are the same as for the 1969 eruption (Ortiz et al., 1987; Smellie, 2002b). We considered particle sizes ranging from -6 to 2 Φ (i.e. 64 mm to 0.25 mm), which cover the entire range of particle sizes observed in the volcanic deposits of the 1970 eruption (González-Ferrán et al., 1971; Shultz, 1972; Pedrazzi et al., 2014). It is clear that, as in the 1967 and 1969 eruptions (Smellie, 2002a), ash fall may also affect the southern part of the island, thereby hindering the exit of ships sailing from inside Port Foster (Fig. 3d). Moreover, as shown in Figure 10, ash fall may even cause problems for vessels operating several kilometres away from

Deception Island.

5.3.2. Lava flows

The lava flow (probabilistic) model applied is based on the assumption that topography and flow thickness play major roles in determining lava paths (Felpeto et al., 2007 and references therein). Input parameters required by the model include a Digital Elevation Model (DEM), maximum flow lengths and height correction (i.e. average thickness of the flow). In the case of Deception Island, simulations were run over a DEM with a cell size of 30 meters. Small lava flows that accumulated near the eruptive vent and did not flow over long distances were generated in the historical eruptions (Smellie, 2002a). The eruption with the largest lava flow was that of 1842, from Mt. Kirkwood, which reaches a maximum length of 5 km. Thus, we assumed flow lengths in the range 1–5 km. The thickness used as input data for the models was 3 m, corresponding to the average value of individual flows measured in the field. The simulations were run for all cells in the DEM and the sum of the 5,000 iterations provided a map with the probability for any particular cell of being covered by a lava flow. Figure 11a consists of a lava-flow simulation probability map, which shows that there is a high probability that the caldera interior around the shores of Port Foster will be affected by lava flows. From this map it is clear that both scientific stations on the island and the evacuation routes proposed by the Spanish military staff (based on logistical criteria) are all located in areas with a moderate-to-high probability of being affected by lava flows.

5.3.3. PDCs

Pyroclastic density currents (PDCs) were simulated using the energy cone model (Sheridan and Malin, 1983) with input parameters of topography, the collapse equivalent height (*Hc*) and angle (θ). The latter is obtained by the arctangent of the ratio between *Hc* and *L*, where *L* represents the run-out length (Felpeto et al., 2007; Toyos et al., 2007). The output of the model is the maximum potential extent that can be affected by the flow (Malin and Sheridan, 1982; Toyos et al., 2007; Felpeto et al., 2007). The collapse equivalent height values range from 100 m up to about 1000 m (for very large eruptions), while the angle values range from about 4º for base surge explosions to 27º for column collapse phases (Sheridan and Malin, 1983). The result of each simulation is the area potentially attainable by a PDC.

On Deception Island, mapped surge deposits extend about 2 km from known vents and are small in volume (Smellie, 2002a). Collapse equivalent heights were chosen in the range of 200–500 m above the possible vent site in order to constrain the best *Hc* matching real deposits. We simulated PDCs with a collapse angle of 12º calculated from the ratio between the *Hc* and the run-out length. Results are shown in Figure 11b. The map obtained represents the sum of the simulation for all cells in the DEM for a collapse column of 400 meters and an inclination of the energy cone of 12º. The map shows how the interior area of Mt. Kirkwood has a high probability of being affected by dilute pyroclastic density currents that would affect the scientific stations and the evacuation routes. In addition, Telefon Ridge has a moderate-high probability of being invaded by PDCs, which would also affect evacuation routes.

5.3.4. Lahars

The LAHARZ semi-empirical code creates hazard-zonation maps that depict estimates of the location and extent of areas inundated by lahars (Hoblitt et al., 1995,

Schilling, 1998). The input parameters of this model are the Digital Elevation Model (DEM) and lahar volume, which provide an automated method for mapping areas of potential lahar inundation.

The lahar eruptive scenario was computed bearing in mind the fact that, in association with subglacial eruptions, lahars affected Deception Island during past activity (Smellie, 2002a, 2002b). Based on the estimated volumes from the 1969 eruption located under the Mt. Pond glacier (Smellie, 2002b), simulations were run with a volume of few millions of m^3 originating along fissures in the two principal glacier zones, Mt. Pond and Mt. Kirkwood (Fig. 2a). These summits have extensive thin glaciers that could represent a significant hazard, creating a large and sudden discharge of melt water that would overflow the glacier.

Figure 11c shows a lahar simulation with hazard gradations ranging from low to high probabilities. The map shows how lahars could flood and reach the sea, and seriously damage the *Gabriel de Castilla* station on the way. From the map it is clear, as in the case of lava flows, that evacuation routes are located in moderate-to-high probability areas.

5.4 Hazard map

Finally, we obtained a qualitative hazard map with four levels of hazard (Fig. 12): very low, low, moderate and high. We established these levels on the basis of a combination of simulations for an area invaded by lava flows, lahars, and PDCs. The map shows that in the interior of the caldera there is mostly a moderate-to-high risk of being affected by one of the hazard scenarios considered. The highest hazard level is confined to the north-eastern flanks of Mt. Kirkwood, Pendulum Cove and the south-eastern slopes of Telefon Ridge (Fig. 12). The few areas with only a very low hazard

level are mainly limited to Baily Head and Entrance Point (Fig. 12). From the hazard map it is clear that the two scientific stations on the island are both located in moderate-to-high hazard zones. Moreover, some of the evacuation routes run through areas possessing very high hazard level.

6. Discussion

Deception Island is the most active volcanic complex in the South Shetland Islands. Despite the important continuous research activity and the increasing number of tourists per year, no detailed hazard assessment has ever been conducted for the island. Two previous attempts have been made: Roobol (1982) mainly focused on assessing the zones threatened by lahars and constructed a model using topographic data and the extent of the ice cap, while Smellie (2002a) basically used observations of the extent of the products from the most recent historical eruptions in 1842, 1967, 1969 and 1970.

It is clear that hazard assessment on Deception Island may be limited by the lack of a complete geological record (e.g. chronological and stratigraphic data). Nonetheless, the threat evaluation and the spatio-temporal analysis presented here do provide a comprehensive hazard assessment for the island. Despite the intrinsic limitations of the methodology (partially due to the scarcity of data), we believe that this first analysis – albeit subject to improvement by new data – represents an important tool in management planning and in preparation for possible evacuations.

Even by assuming conservative values for some of the evaluated factors, the threat score obtained using the NVEWS test (Ewert et al., 2005) gives a range of 107.2–180, which places Deception island in the category of a volcano with a high-to-very-high threat, comparable to Crater Lake, St. Helens, Novarupta and Katmai in the USA (Ewert et al., 2005). According to Ewert et al. (2005), these high-threat volcanoes

should be closely monitored in real-time. In more detail, the monitoring network must be able to track changes occurring in the system as they happen and to apply models to the on-going and expected activity. On Deception Island, Spanish seismologists monitor the island with five seismometers and one array during the austral summer (Carmona et al., 2012). During some campaigns other scientific groups also measure ground deformation and temperature (e.g. Prates et al., 2013; Peci et al., 2014). In light of the NVEWS recommendations, the volcano-monitoring network on Deception Island should be improved, especially considering the important tourist and scientific activity ocurring during the Antarctic summer..

The present hazard assessment is relevant as an analysis of the adequacy of the current evacuation routes and locations of the active scientific stations. From Figure 12, it is clear that both *Base Decepcion* and *Gabriel de Castilla* station are located in areas of moderate to high hazard. Previous work dealing with hazard assessment on Deception Island have already advised against the construction of permanent buildings on the shores of Port Foster (Roobol, 1982; Smellie, 2002a). Baker and co-authors (1975) highlighted that it would be "evidently unwise" to construct any new stations or any other kind of installation on the island. Roobol (1982) proposed that the safest place would be along Kendall Terrace outside the ring-fault zone (Fig. 5a) and argued that, if two different constructions were installed there, it seemed extremely unlikely that one would not survive the other in case of an eruption. Figure 12 demonstrates that the destroyed Chilean and British stations were, indeed,

located in areas with high hazard level.

As is clearly suggested by the range of volcanic hazards identified on Deception Island, and given the increasing number of tourists and scientific expeditions visiting the island and its surroundings, it is important to identify escape routes in case of a sudden volcanic eruption. The escape strategy provided by the Spanish military staff is illustrated in Figure 12. However, the evacuation routes from both scientific stations run through zones with high hazard level. Indeed, as Smellie (2002a) remarks, all possible escape routes from the inner bay to the outer coast are demanding since they include climbing up on to the steep caldera walls. So, because the routes are physically arduous, even fit persons may end exhausted. It should be added that it is almost impossible to use ground vehicles to transport people and, if possible, considerable skill and local knowledge of the routes are required (cf. Smellie, 2002a).

All routes to the outer coast would take hours to complete – a minimum of two hours for the easiest route (Fig. 12, label 1) and over three or four hours (or more) for the most difficult ones (Fig. 12, label 2). According to Smellie (2002a), there are no recommended safe routes over snow and ice because the inherent difficulties of travelling over glaciers (e.g. crevasses, whiteout, slippery surfaces). So, glacier travel should be avoided unless with trained guides using suitable equipment, although this is unlikely to be readily available in an emergency (cf. Smellie, 2002a). It should be added that the existing evacuation routes shown in Figure 12 were defined without any accurate hazard assessment and taking into account only logistical considerations. Thus, the results presented here should encourage a revision of the distribution and course of the evacuation routes.

The evacuation of the island would be difficult for a number of other reasons. First, it is possible that the entrance to Port Foster would be blocked or difficult to sail

through due to the eruption, a tsunamis or any other of the hazards outlined here. Thus, all ships present within the bay when an eruption begins should set sail immediately, preferably after uplifting all people on the ground (Smellie, 2002a). Vessels should also avoid sailing too close to Cathedral Crags given the possibility of rock falls from these unstable cliffs.

Another aspect to be taken into account is that all rescue ships and helicopters should avoid passing through or under the eruption ash cloud due to the possibility of damage to machinery caused by ash particles. This is an important difficulty during rescue operations given that the hazard assessment developed in this study and, above all, the eruptive simulations reveal the possibility that Neptune's Bellows will be affected by ash fall. This would hamper any rescue operation and navigation routes, as well as activity on other islands. On the other hand, PDCs and lava flows are more constrained to the area around the vents, but these could still affect the research stations and create a problem for the existing evacuation routes.

7. Conclusions

Here we present a long-term volcanic hazard assessment of Deception Island that takes into account both temporal and spatial probabilities. The computation of the latter probabilities for the different eruptive scenarios is important in the evaluation of the hazard level on different parts of the island. These values can be easily updated and improved with the incorporation of new information such as a more complete volcanic stratigraphy and geochronological data.

The hazard probability map shows that the research stations could be affected by PDCs and that a large area of the island could be covered by ash fallout. Furthermore, the opening of new fissures in the glacier zones could generate lahars that would reach

the research stations and affect evacuation routes. These results are useful for planning and choosing suitable routes for evacuating the island during a volcanic crisis in the Antarctic summer when the island is populated.

Finally, it is worth mentioning that this long-term assessment may help decision makers when faced with difficult situations such as the allocation of resources for hazard prevention and evacuation whose objective is to reduce the loss of life due to the potential impact of volcanic hazards.

Acknowledgements

This work was supported by the European Commission (FP7 Theme: ENV.2011.1.3.3-1; Grant 282759: VUELCO) and the MICINN grant CTM2011-13578-E. AG is grateful for her Juan de la Cierva Grant (JCI-2010-06092) and Ramón y Cajal contract (RYC-2012-11024). We would like to thank all the military staff from the Spanish Antarctic Base *Gabriel de Castilla* for their constant help and for the logistic support, without which this research would have been impossible. We would also like to thank Manuel Bañón for his help with the meteorological information. The authors are grateful to two anonymous reviewers for their insightful comments and review of the manuscript, which has helped us improve this work. We also thank the Editor Lionel Wilson for handling this paper. The English text was corrected by Michael Lockwood.

References

Aristarain, A.J., Delmas, R.J., 1998. Ice record of a large eruption of Deception Island Volcano (Antarctica) in the XVIITH century. J. Volcanol. Geotherm. Res. 80, 17-25.

Aspinall, W. P., Woo, G., 1994. An impartial decision-making proce- dure using expert judgment to assess volcanic hazards, in Large Explosive Eruptions. Accad. Naz. dei Lincei, Rome. Atti Conv. Lincei 112, 211-220.

Aspinall, W.P., 2006. Structured elicitation of expert judgment for probabilistic hazard and risk assessment in volcanic eruptions. In: Mader, H.M., Coles, S.G., Connor, C.B., Connor, L.J. (Eds.), Statistics in Volcanology. : Special Publication of IAVCEI, 1. Geol. Soc. London, pp. 15–30.

Baker. P.E., McReath, I., Harvey. M.R., Roobol, M.J., Davies. T.G., 1975. The geology of the South Shetland Islands: V. Volcanic evolution of Deception Island. Br. Antarct. Surv. Sci. Rep., 78-81.

Bartolini, S., Cappello, A., Martí, J., Del Negro, C., 2013. QVAST: a new Quantum GIS plugin for estimating volcanic susceptibility. Nat. Hazards Earth Syst. Sci. 13, 3031–3042.

Becerril, L., Cappello, A., Galindo, I., Neri, M., Del Negro, C., 2013. Spatial probability distribution of future volcanic eruptions at El Hierro Island (Canary Islands, Spain). J. Volcanol. Geotherm. Res. 257, 21-30.

Becerril, L., Bartolini, S., Sobradelo, R., Martí, J., Morales, J. M., Galindo, I., 2014. Long-term volcanic hazard assessment on El Hierro (Canary Islands). Nat. Hazards Earth Syst. Sci. 14, 1853-1870.

Birkenmajer, K. 1991. Lichenometric dating of a mid_19th century lava eruption at Deception Island (West Antarctica). Bulletin of the Polish Academy of Science, Earth Sciences 39, 1-9.

Björck, S., Sandgren, P. y Zale, R., 1991. Late Holocene tephrochronology of the Northern Antarctic Peninsula. Quaternary Research 36, 322-328.

Cappello, A., Neri, M., Acocella, V., Gallo, G., Vicari, A., Del Negro, C., 2012. Spatial vent opening probability map of Etna volcano (Sicily, Italy). Bull. Volcanol. 74, 2083-2094.

Cappello, A., Bilotta, G., Neri, M., Del Negro, C., 2013. Probabilistic modeling of future volcanic eruptions at Mount Etna. J. Geophys. Res. Solid Earth 118, 1-11.

Carmona, E., Almendros, J., Martín, R., Cortés, G., Alguacil, G., Moreno, J., Martín, B., Martos, A., Serrano, I., Stich, D., Ibáñez, J.M., 2012. Avances y mejoras en el monitoreo sísmico de Isla Decepción (Antártida). Proceedings de la 7ª Asamblea Hispano-Portuguesa de Geodesia y Geofísica, pp. 267- 271.

Caselli, A.T., Agusto, M.R., 2004. Recent hydrovolcanic deposits with evidence of magmatic immiscibility on Deception Island, Antarctica. Depósitos hidrovolcánicos recientes con indicios de inmiscibilidad magmática en la isla Decepción (Antártida). Rev. Asoc. Geol. Argent. 59(3), 495-500.

Connor, C.B., Hill, B.E., 1995. Three nonhomogenous Poisson models for the probability of basaltic volcanism: application to the Yucca Mountain region, Nevada. J. Geophys. Res. 100(B6), 107–110.

Connor, L.J., Connor, C.B., Meliksetian, K., Savov, I., 2012. Probabilistic approach to modeling lava flow inundation: a lava flow hazard assessment for a nuclear facility in Armenia. J. Appl. Volcanol. 1(3), 1-19.

Delmas, R.J., 1992. Environmental information from ice cores. Rev. Geophys. 30, I-21.

Diggle, P. J., 1985. A kernel method for smoothing point process data. Applied Statistics, J. R. Stat. Soc. Ser. C. 34, 138–147.

Ewert, J., Guffanti, M., Murray, T., 2005. An assessment of volcanic threat and monitoring capabilities in the United States: Framework for a National Volcanic Early Warning System, NVEWS. US Geoll. Sur. Open-File Rep. 1164, 1–62.

Felpeto, A., Martí, J., Ortiz, R., 2007. Automatic GIS-based system for volcanic hazard assessment. J. Volcanol. Geotherm. Res. 166, 106–116.

Fernández-Ibañez, F., Perez-Lopez, R., Martinez-Diaz, J.J., Paredes, C., Giner-Robles, J.L., Caselli, A.T., Ibañez, J.M., 2005. Costa Recta beach, Deception Island, West Antarctica: a retreated scarp of a submarine fault. Antarctic Sci. 17, 418–426.

Folch, A., Felpeto, A., 2005. A coupled model for dispersal of tephra during sustained explosive eruptions. J. Volcanol. Geotherm. Res. 145, 337–349.

Fretzdorff, S., Smellie, J.L., 2002. Electron microprobe characterization of ash layers in sediments from the central Bransfield basin (Antarctic Peninsula): evidence for at least two volcanic sources. Antarctic Sci. 14(4), 412-421.

González-Ferrán, O., Munizaga, F., Moreno, H., 1971. Síntesis de la evolución volcánica de la isla Decepción y la erupción de 1970. Instituto Antártico Chileno, Serie Científica 2(1), 1-14.

González-Ferrán, O., 1985. Volcanic and tectonic evolution of the northern Antarctic Peninsula - Late Cenozoic to Recent. In: Husebye, E.S., Johnson, G.L. Kristoffersen, Y. (Eds.), Geophysics of the Polar Regions, Tectonophysics, 114, pp. 389-409.

Gottsmann, J., Folch, A., Rymer, H., 2006. Unrest at Campi Flegrei: a

contribution to the magmatic versus hydrothermal debate from inverse and finite element modelling. J. Geophys. Res. 111, B07203.

Gottsmann, J., Carniel, R., Coppo, N., Wooller, L., Hautman, S., Rymer, H., 2007. Oscillations in hydrothermal systems as a source of periodic unrest at caldera volcanoes: multiparameter insights from Nisyros, Greece. Geophys. Res. Lett. 34, L07307.

Grad, M., Guterch, A., Sroda, P., 1992. Upper crustal structure of Deception Island area, Bransfield Strait, West Antarctica. Antarctic Sci. 4, 469-476.

Hawkes, D.D., 1961. The geology of the South Shetland Islands: II. The geology and petrology of Deception Island. Falkland Islands Dependencies Survey Scientific Reports 27, 43.

Hoblitt, R.P., Walder, J.S., Driedger, C.L., Scott, K.M., Pringle, J.T., Vallance, J.W., 1995. Volcano hazards from Mount Rainier, Washington. U.S. Geological Survey Open-File Report 95- 273, pp. 10.

Hodgson, A.D., Dyson, C.L., Jones, V.J. & Smellie, J.L. 1998. Tephra analysis of sediments from Midge Lake (South Shetland Islands) and Sombre Lake (South Orkney Islands), Antarctica. Antarctic Sci. 10, 13-20.

Ibañez, J., Almendros, J., Carmona, E., Martínez-Arévalo, C., Abril, M., 2003. The recent seismo-volcanic activity at Deception Island volcano. Deep-Sea Res. II 50, 1611–1629.

Keller, R.A., Fisk, M.R., White, W.M., Birkenmajer, K., 1992. Isotopic and trace element constraints on mixing and melting models of marginal basin volcanism, Bransfield Strait, Antarctica. Earth Planet Sci. Lett. 111, 287–303.

Kendall, E.N. 1831. An account of the Island of Deception, one of the New Shetland Isles. Extracted from the private journal of Lieutenant Kendal, R.N., embarked

on board his Majesty's sloop CJumticieer, Captain Foster, on a scientific voyage; and communicated by John Barrow, Esq., F.R.S. Journal of the Royal Geographical Society, London 1, 62-66.

Kinvig, H.S., Winson, A., Gottsmann, J., 2010. Analysis of volcanic threat from Nisyros Island, Greece, with implications for aviation and population exposure. Nat. Hazards Earth Syst. Sci. 10, 1101–1113.

López-Martínez, J., Serrano, E., Rey, J., Smellie, J.L., 2000. Geomorphological map of Deception Island. BAS GEOMAP Series, Sheet 6-B, 1:25,000. Br. Antarct. Surv., Cambridge.

Lutz, T. M., Gutmann, J. T., 1995. An improved method for determining and characterizing alignments of point-like features and its implications for the Pinacate volcanic field, Sonoran, Mexico. J. Geophys. Res. 100, 17659–17670.

Maestro, A., Somoza, L., Rey, J., Martinez-Frias, J., Lopez-Martinez, J., 2007. Active tectonics, fault patterns, and stress field of Deception Island: a response to oblique convergence between the Pacific and Antarctic plates. Jour. South Am. Earth Sci. 23, 256–268.

Malin, M.C., Sheridan, M.F., 1982. Computer-assisted mapping of pyroclastic surges. Science 217, 637–640.

Martí, J., Aspinall, W., Sobradelo, R., Felpeto, A., Geyer, A., Ortiz, R., Baxter, P., Cole, P., Pacheco, J., Blanco, M., Lopez, C., 2008. A long-term volcanic hazard event tree for Teide-Pico Viejo stratovolcanoes (Tenerife, Canary Islands). J. Volcanol. Geotherm. Res. 178(3), 543-552.

Martí, J., Felpeto, A., 2010. Methodology for the computation of volcanic susceptibility: Application to Tenerife Island (Canary Islands). J. Volcanol. Geotherm. Res. 195, 69-77.

Martí, J., Sobradelo, R., Felpeto, A., García, O., 2012. Eruptive scenarios of phonolitic volcanism at Teide-Pico Viejo volcanic complex (Tenerife, Canary Islands). Bull. Volcanol. 74, 767–782.

Martí, J., Geyer, A., Aguirre-Diaz, G., 2013. Origin and evolution of the Deception Island caldera (South Shetland Islands, Antarctica). Bull. Volcanol. 75, 732.

Martin, A.J., Umeda, K., Connor, C.B., Weller, J.N., Zhao, D., Takahashi, M., 2004. Modeling long-term volcanic hazards through Bayesian inference: an example from the Tohuku volcanic arc Japan, J. Geophys. Res. 109, B10208.

Marzocchi, W., Sandri, L., Selva, J., 2008. BET EF: a probabilistic tool for long- and short-term eruption forecasting. Bull. Volcanol. 70(5), 623–632.

Marzocchi, W., Sandri, L., Selva, J., 2010. BET VH: a probabilistic tool for long-term volcanic hazard assessment. Bull. Volcanol. 72, 705–716.

Mathies, D., Mäusbacher, R. y Storzer, D., 1990. Deception Island tephra : a stratographical marker for limnic and marine sediments in Bransfield Strait area, Antarctica. Zentralbl. Geol. Paläontol. Teil (1-2), 153-165.

Moreton, S.G., Smellie, J.L., 1998. Identification and correlation of distal tephra layer; in deep-sea sediment cores, Scotia Sea, Antarctica. Annals of Glaciology 27, 285-289.

Moreton, S.C., 1999. Quaternary tephrochronology of the Scotia Sea and Bellingshausen Sea, Antarctica. Ph.D. thesis, Cheltenham and Gloucester College of Higher Education, pp. 164, unpublished.

Neri, A., Aspinall, W.P., Cioni, R., Bertagnini, A., Baxter, P.J., Zuccaro, G., Andronico, D., Barsotti, S., Cole, P.D., Esposti Ongaro, T., Hincks, T.K., Macedonio, G., Papale, P., Rosi, M., Santacroce, R., Woo, G., 2008. Developing an event tree for probabilistic hazard and risk assessment at Vesuvius. J. Volcanol. Geotherm. Res.

178(3), 397-415.

Newhall, C. G., Hoblitt, R. P., 2002. Constructing event trees for volcanic crisis. Bull. Volcanol. 64, 3–20.

Orheim, O., 1972. A 200-year record of glacier mass balance at Deception Island, southwest Atlantic Ocean, and its bearing on models of global climate change, Institute of Polar Studies, Ohio State University, 118.

Ortiz, R., Araña, V., Vila, J., Viramonte, J.G., Mazzuoli, R., 1987. Mecanismos de erupción de la reciente actividad volcánica en Decepción, Actas II Simposio Español de Estudios Antárticos, CSIC, 217–227.

Palais, J.M., Kirchner, S., Delmas, R., 1989. Identification and correlation of volcanic eruption horizons in a 1000 year ice-core record from the South Pole. Antarctic Journal US Review 24, 101-104.

Pallàs, R., Smellie, J.L., Casas, J.M. and Calvet, J., 2001. Using tephrochronology to date temperate ice: correlation between ice tephras on Livingston Island and eruptive units on Deception Island volcano (South Shetland Islands, Antarctica). The Holocene 11(2), 149-160.

Patrick, M., Smellie, J.L., 2013. Synthesis. A spaceborne inventory of volcanic activity in Antarctica and southern oceans, 2000–10. Antarctic Sci. 25(4), 475–500.

Peccerillo, A., Tripodo, A., Villari, L., Currieri, S., Zimbalaiti, E., 1991. Genesis and evolution of volcanism in back-arc areas. A case history, the Island of Deception (Western Antarctica). Periodico di Mineralogia 60, 29-44.

Pedrazzi, D., Aguirre Díaz, G., Bartolini, S., Martí, J., Geyer, A., 2014. The 1970 eruption on Deception Island (Antarctica): eruptive dynamics and implications for volcanic hazards. J. Geol. Soc. London, in press.

Peci, L.M., Berrocoso, M., Fernández-Ros, A., García, A., Marrero, J.M., Ortiz,

R., 2014. Embedded ARM System for Volcano Monitoring in Remote Areas: Application to the Active Volcano on Deception Island (Antarctica). Sensors 14, 672-690.

Prates, G., Berrocoso, M., Fernández-Ros, A., García, A., 2013. Enhancement of sub-daily positioning solutions for surface deformation monitoring at Deception volcano (South Shetland Islands, Antarctica). Bull. Volcanol. 75(2), 1-10.

Ramos, M., Ortiz, R., Diez-Gil, J.L., Viramonte, J., 1989. Anomalias térmicas y balance de flujo energético sobre el suelo del volcän Decepción, Isla Decepción (Shetland del Sur). Actas del III Simposium Español de Estudios Antárticos, CSIC, 203-219.

Rey, J., Somoza, L., Martínez-Frías, J., 1995. Tectonic, volcanic, and hydrothermal event sequence on Deception Island (Antarctica). Geo Mar. Lett. 15, 1–8.

Roach, P.J., 1978. The nature of back-arc extension in Bransfield Basin. Geophys. J. Royal Astron. Soc. 53, 165.

Roobol, M.J., 1973. Historic volcanic activity at Deception Island. Br. Antarct. Surv. Bull. 32, 23-30.

Roobol, M.J., 1980 (for 1979). A model for the eruptive mechanism of Deception Island from 1820 to 1970. Br. Antarct. Surv. Bull. 49, 137-156.

Roobol, M.J., 1982. The volcanic hazard at Deception Island, South Shetland Islands. Br. Antarct. Surv. Bull. 51, 237-245.

Schilling, S.P., 1998. LAHARZ: GIS program for automated mapping of lahar-inundation hazard zones. U.S. Geological Survey Open-File Report, pp. 98-638

Sheridan, M. F., Malin, M. C., 1983. Application of computer-assisted mapping to volcanic hazard evaluation of surge eruption: Vulcano, Lipari, Vesuvius, explosive volcanism. J. Volcanol. Geotherm. Res. 17, 187–202.

Shultz, C.H., 1972. Eruption at Deception Island, Antarctica, August 1970. Geol. Soc. Am. Bull. 83(9), 2837-2842.

Smellie, J.L., 1988. Recent observations on the volcanic history of Deception Island, South Shetland Islands. Br. Antarct. Surv. Bull. 81, 83–85.

Smellie, J.L., 1999. The upper Cenozoic tephra record in the south polar region: a review. Glob. Planet Chang. 21, 51–70.

Smellie, J.L., 2001. Lithostratigraphy and volcanic evolution of Deception Island, South Shetland Islands. Antarctic Sci. 13, 188–209.

Smellie, J.L., 2002a. Volcanic hazard. In: López-Martínez, J., Smellie, J.L., Thomson, J.W., Thomson, M.R.A. (Eds.), Geology and geomorphology of Deception Island. Cambridge, Br. Antarct. Surv., Natural Environmental Research Council 2002, pp. 47-53.

Smellie, J.L., 2002b. The 1969 subglacial eruption on Deception Island (Antarctica): events and processes during an eruption beneath a thin glacier and implications for volcanic hazards. Volcano-Ice Interactions on Earth and Mars. Geol. Soc. London, Special Publications 202, 59-79.

Smellie, J.L., López-Martínez, J., 2002. Introduction. In: López-Martínez, J., Smellie, J.L., Thomson, J.W., Thomson, M.R.A. (Eds.), Geology and geomorphology of Deception Island. Cambridge, British Antarctic Survey, Natural Environmental Research Council 2002, pp. 1-6.

Smellie, J.L., López-Martínez, J., and others, 2002. Geology and geomorphology of Deception Island. BAS GEOMAP series, Sheets 6-A and 6-B, 1:25 000. Cambridge, Br. Antarct. Surv., Cambridge, pp. 78.

Smith Jr.a, K.L., Baldwina, R.J., Glattsa, R.C., Chereskinb, T.K., Ruhla, H., Lagunc, V., 2003. Weather, ice, and snow conditions at Deception Island, Antarctica:

long time-series photographic monitoring. Deep-Sea Research II 50, 1649–1664.

Sobradelo, R., Martí, J., 2010. Bayesian event tree for long-term volcanic hazard assessment: Application to Teide-Pico Viejo stratovolcanoes, Tenerife, Canary Islands. J. Geophys. Res. 115, B05206.

Sobradelo, R., Bartolini, S., and Martí, J., 2014. HASSET: a probability event tree tool to valuate future volcanic scenarios using Bayesian inference presented as a plugin for QGIS. Bull. Volcanol. 76, 770.

Suzuki, T., 1983. A Theoretical Model for Dispersion of Tephra. In: Shimozuru, D., Yokoyama, I. (Eds.), Arc Volcanism, Physics and Tectonics. Terra Scientific Publishing Company, Tokyo.

Torrecillas, C., Berrocoso, M. and García-García, A., 2006. The Multidisciplinary Scientific Information Support System (SIMAC) for Deception Island. In: D. Fütterer, D. Damaske, G. Kleinschmidt, H. Miller and F. Tessensohn (Editors), Antarctica. Springer Berlin Heidelberg, pp. 397-402.

Toyos, G. P., Cole, P. D., Felpeto, A., Martí, J., 2007. A GIS-based methodology for hazard map- ping of small pyroclastic density currents. Nat. Hazards 41, 99–112.

Turner, J., Pendlebury, S., 2004. The International Antarctic Weather Forecasting Handbook. Br. Antarct. Surv., Cambridge.

Valencio, A., Mendía, E. and Vilas, J., 1979. Palaeomagnetism and K-Ar age of Mesozoic and Cenozoic igneous rocks from Antarctica. Earth Planet. Sci. Lett. 45, 61-68.

Valenzuela, E., Chávez, L., Munizaga, F., 1970. Actividad volcánica en isla Decepción, Antártica, 1967. Instituto Antártico Chileno Serie 1, 5-16.

Wilkes, C., 1845. American Exploring Expedition: Narrative of the United States Exploring Expedition during the years 18384842 I-V, Lea and Blanchard, Philadelphia.

Woo, G., 1999. The mathematics of natural catastrophes. Imperial College Press, London.

Zandomeneghi, D., Barclay, A., Almendros, J., Ibáñez, J.M., Wilcock, W.S.D., Ben-Zvi, T., 2009. The crustal structure of Deception Island Volcano from P wave seismic tomography: tectonic and volcanic implications. J. Geophys. Res. 11, B06310.

Figure captions

Figure 1: a) Simplified regional tectonic map and location of the South Shetland Islands (modified from Ibañez et al., 2003). HFZ: Hero Fracture Zone, SFZ: Shetland Fracture Zone. b) Location of Deception Island (modified from Grad et al., 1992). Black and white dots indicate nearby year-round and temporary (only austral summer) research stations, respectively. Grey dots correspond to temporary field camps.

Figure 2: a) Simplified geological and tectonic map of Deception Island modified from Martí et al. (2013) and Smellie et al. (2002). b) The sites of the historical volcanic vents, observable fumarolic activity and heated ground are also indicated (data obtained from Spatial Data Infrastructure for Deception Island SIMAC, http://www.simac.uca.es, Torrecillas et al., 2006). As well as the historical vents, we have identified the post-caldera craters that, while not directly related to historical volcanic eruptions, clearly correspond to post-caldera volcanism.

Figure 3: Remains of the British (a) and Chilean (b) bases in Whalers Bay and Pendulum Cove, respectively (see Fig. 2b for exact locations). Remains of the Norwegian whaling station in Whalers Bay (c). Current Spanish *Gabriel de Castilla* (e) and Argentinian *Base Decepcion* (f) scientific bases (see Fig. 2 for exact locations). (d) Photograph of a tourist cruise ship entering Port Foster through Neptune's Bellows. (Authors: A. Villaseñor (a), (b) and (d); J. Galeano (c), (e) and (f)).

Figure 4: a) Visitors to Antarctica during the austral summers over the past two decades. b) Amount of visitors to specific Deception Island sites over the last five years

(source: International Association of Antarctica Tour Operators (IAATO, http://www.iaato.org).

Figure 5: Hazard maps presented by Roobol (1982) (a) and Smellie (2002a) (b).

Figure 6: Flow chart for the volcanic hazard assessment. Tools used in this study are also indicated.

Figure7: Susceptibility map of future eruptions on Deception Island calculated with QVAST (Bartolini et al., 2013).

Figure 8: Bayesian event tree structure for Deception Island including results for the probability estimate using the HASSET tool (Sobradelo et al., 2014).

Figure 9: Sectors on Deception Island based on volcanic susceptibility and topographic criteria. The probabilities of the different hazards in each zone of Deception Island obtained with the application HASSET (Sobradelo et al., 2014) are also shown (see text for more explanation).

Figure 10: Ash fallout simulations with a 5-km column height and volume of 0.3 km^3. All four seasons are simulated using wind data from the *Bellinghsausen* station.

Figure 11: Lava flow (a), PDC (b) and lahar (c) simulation probability maps. Evacuation routes provided by the Spanish military staff are indicated by dotted lines.

Figure 12: Qualitative hazard map for Deception Island. The evacuation routes provided by the Spanish military staff and the best sites for helicopter uplift according to Smellie (2002a) are also indicated.

Table captions

Table 1: Principal characteristics of the volcanic eruptions and unrest periods recorded over the last 372 years (1641–2013). Only eruptions of known age and consistent with the relative field stratigraphy established in this study are included. Information about the nodes in the HASSET tool (Sobradelo et al., 2014) is also included. See text for more details.

Table 2: Additional geochronological data about the recorded volcanic eruptions on Deception Island between 35,400 B.P. and 450 B.P. This information provides the main characteristics of the eruptive style of the island for the application of the Bayesian Event Tree method.

Table 3: Deception Island NVEWS (National Volcano Early Warning System) scoring factors.

Table 4: Bandwidth parameters for all the available datasets on Deception Island obtained using the modified LSCV (Least Square Cross Validation) method (Cappello et al., 2013) in the QVAST tool (Bartolini et al., 2013).

Table 5: Input data for HASSET (Sobradelo et al., 2014). Prior weights and data weights are estimated using data on Deception Island volcanic activity. Past data are based on the eruptions recorded over the last 372 years.

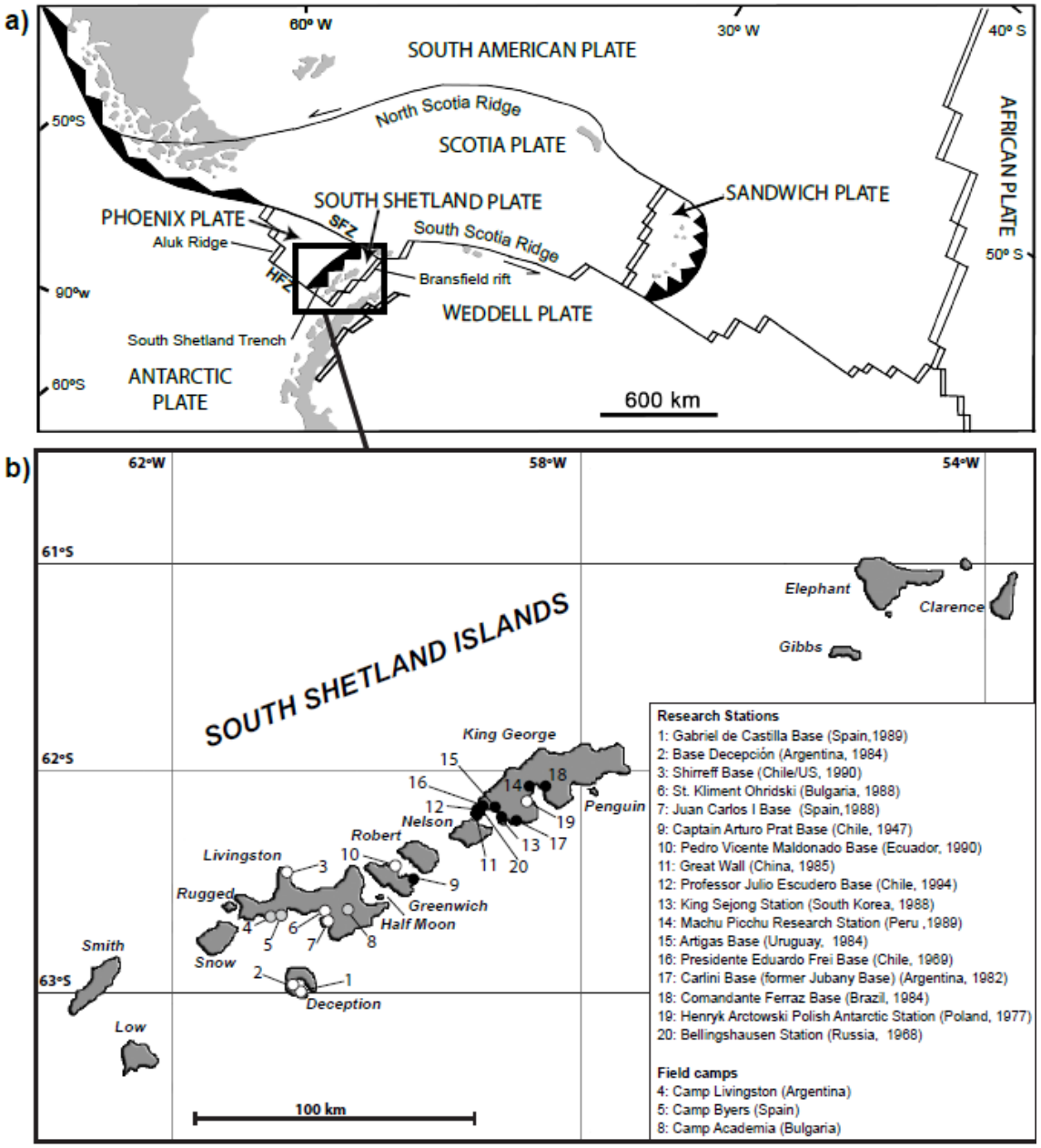

Figure 1

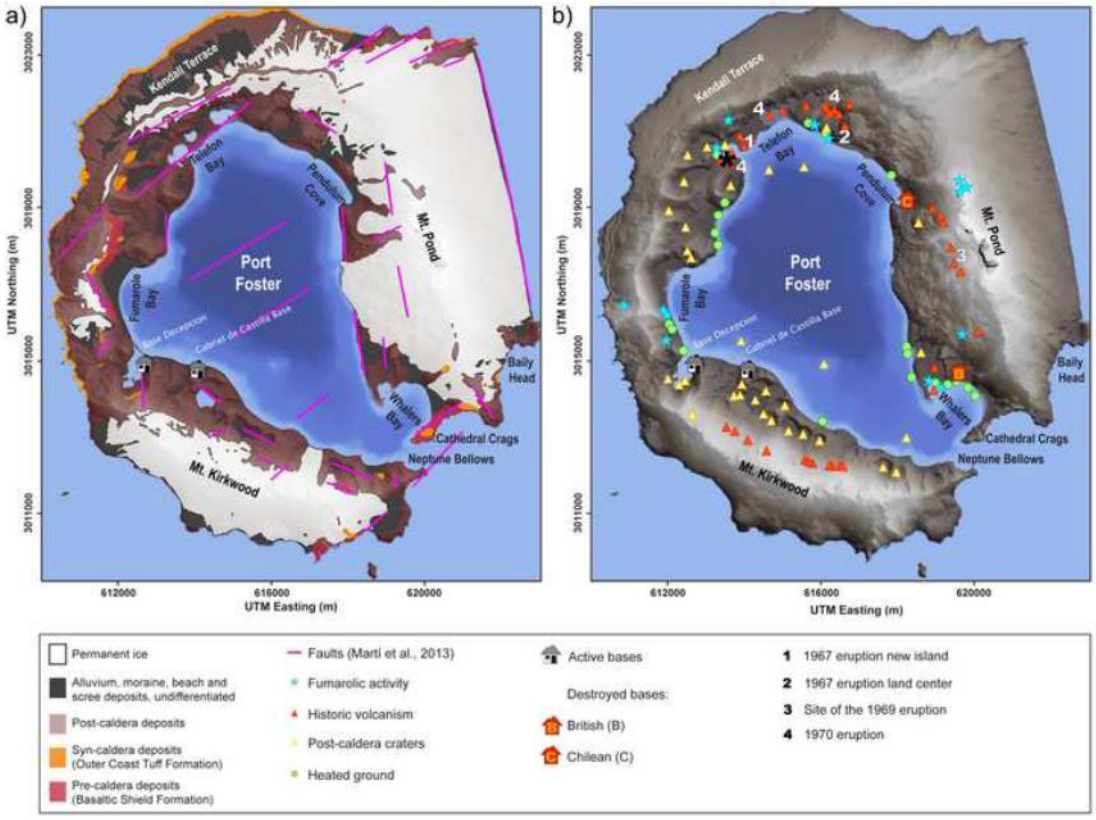

Figure 2

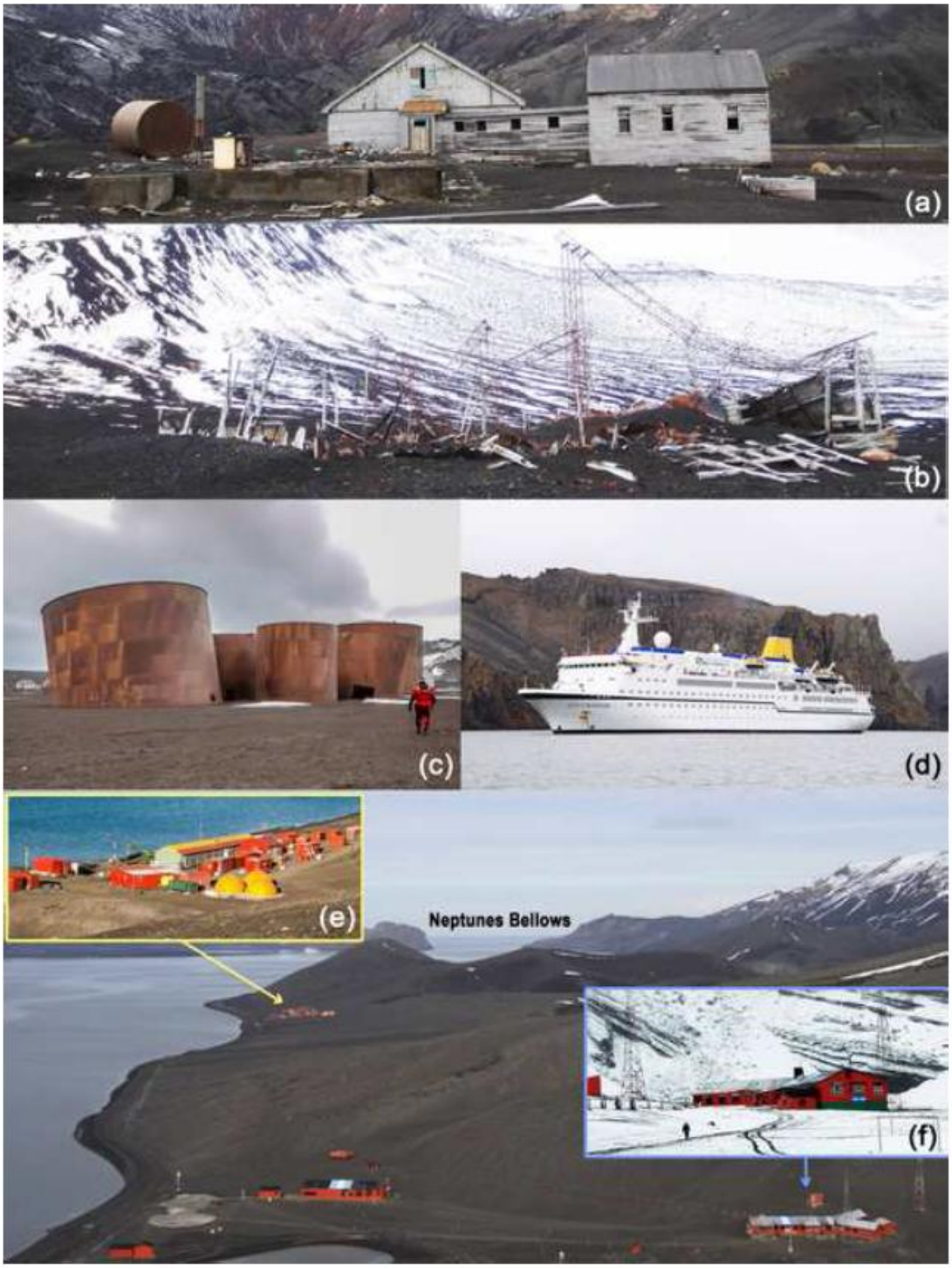

Figure 3

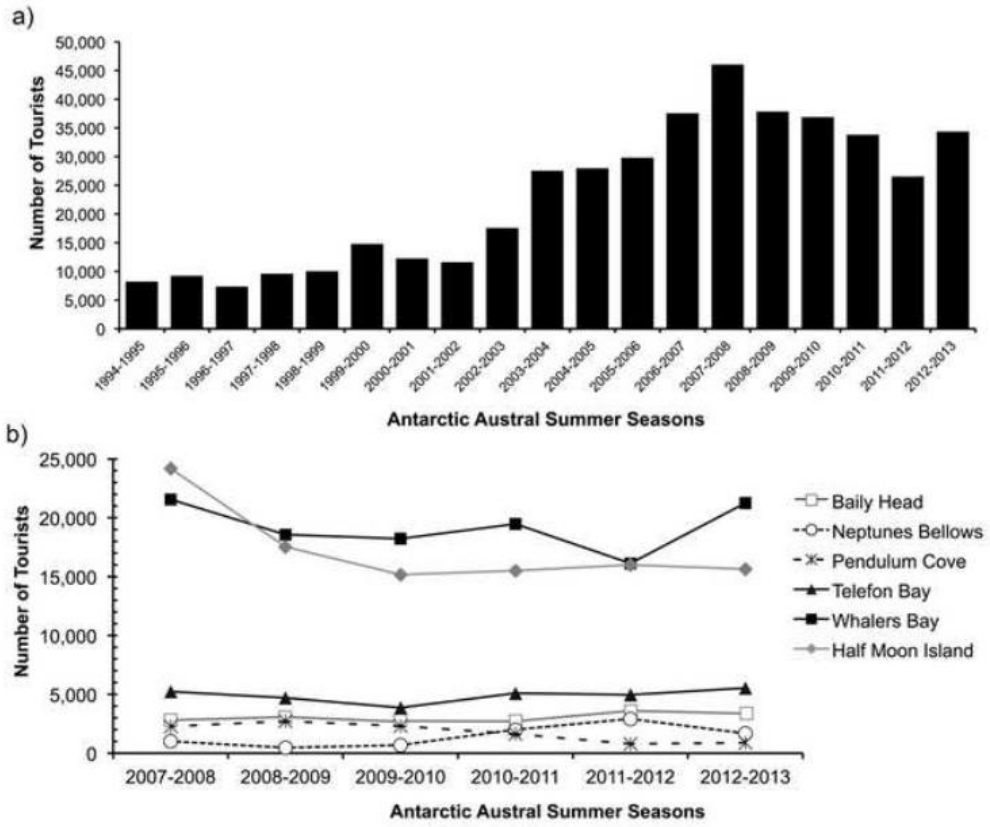

Figure 4

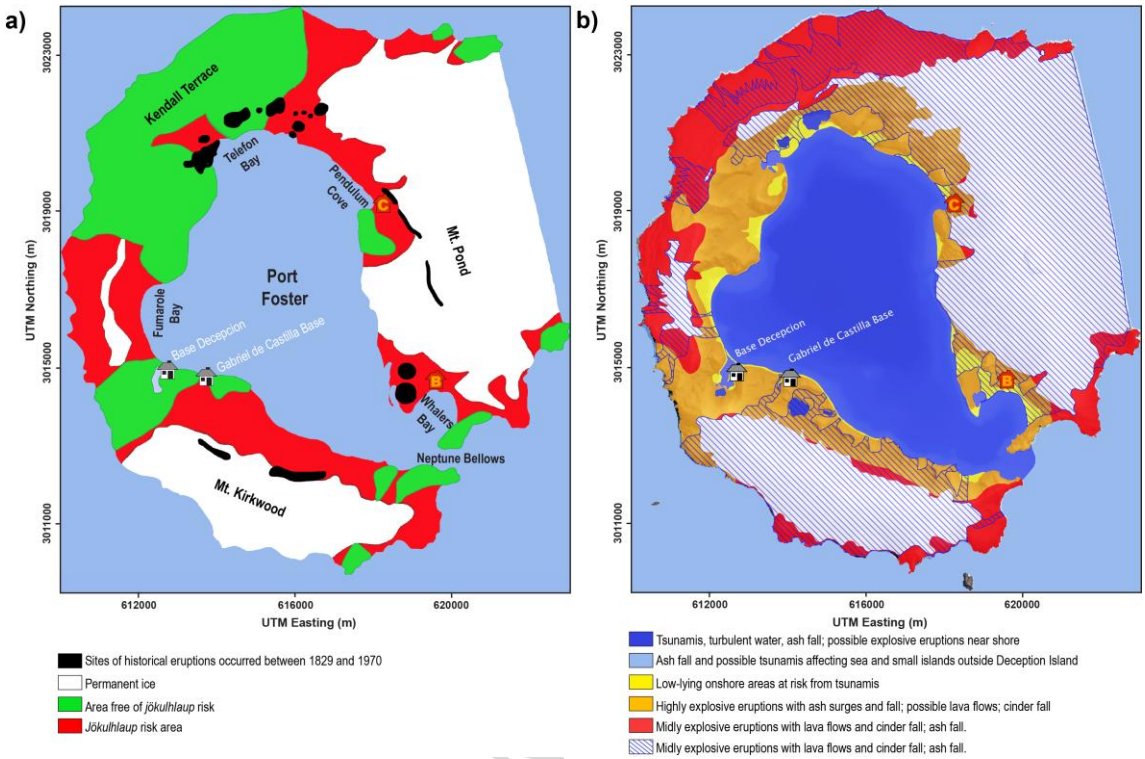

Figure 5

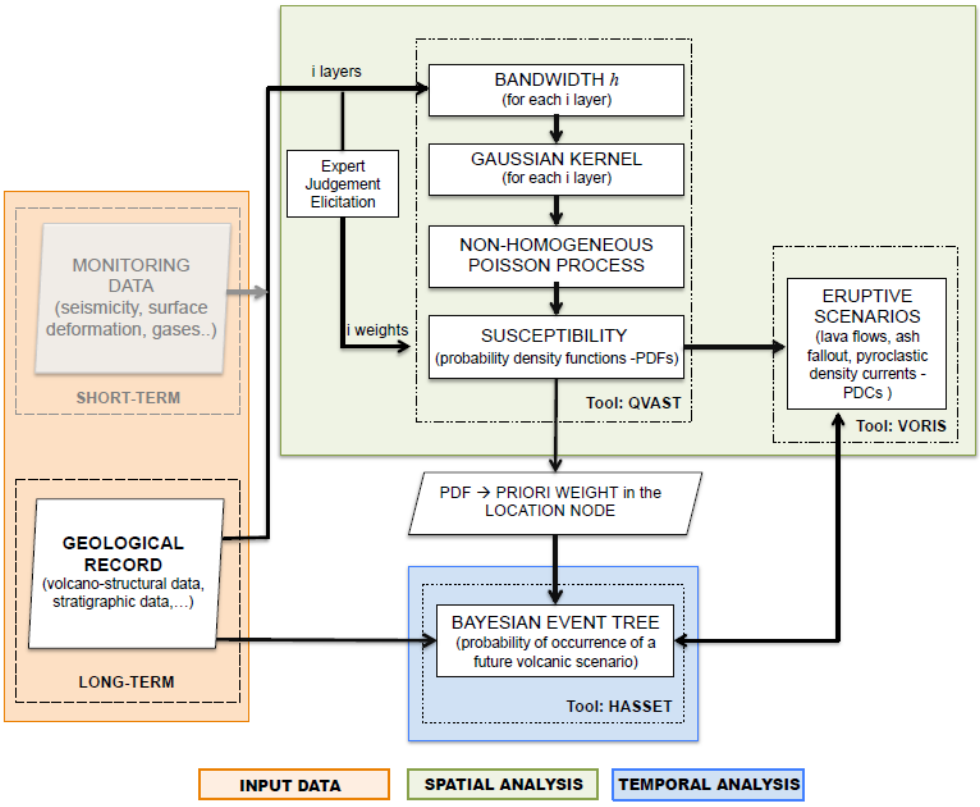

Figure 6

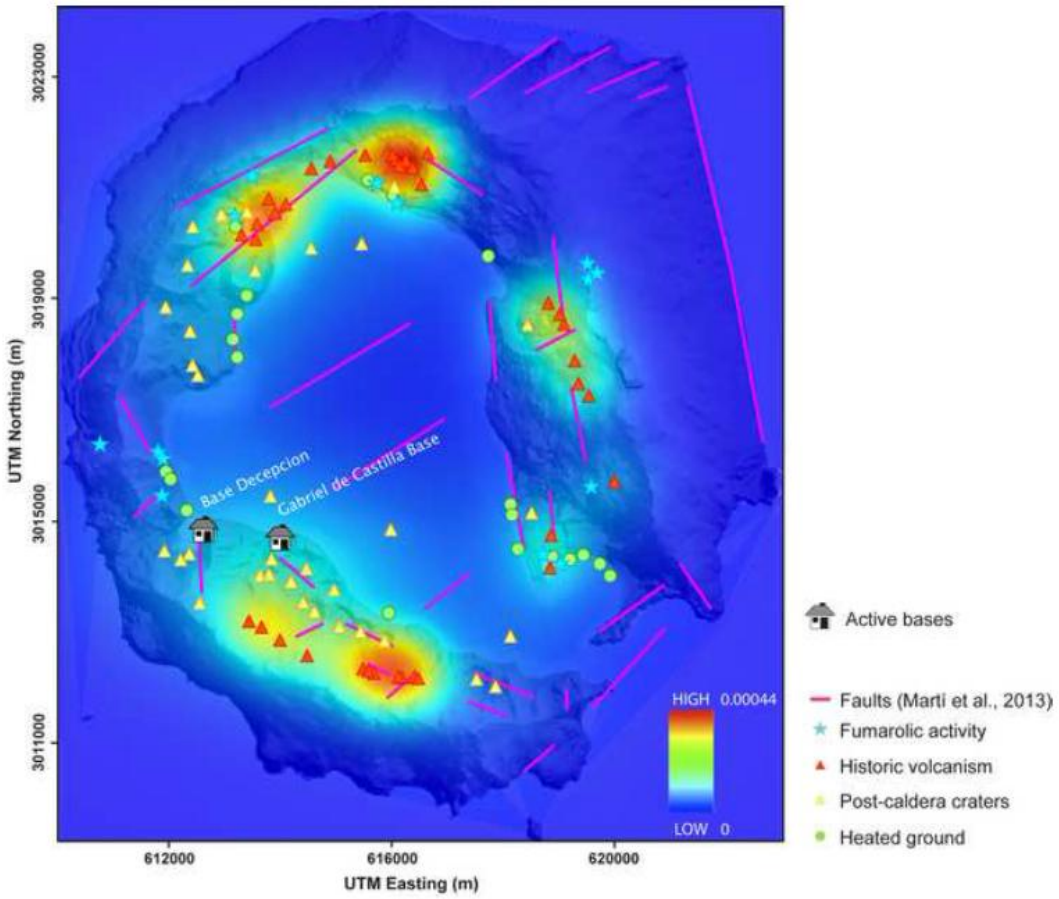

Figure 7

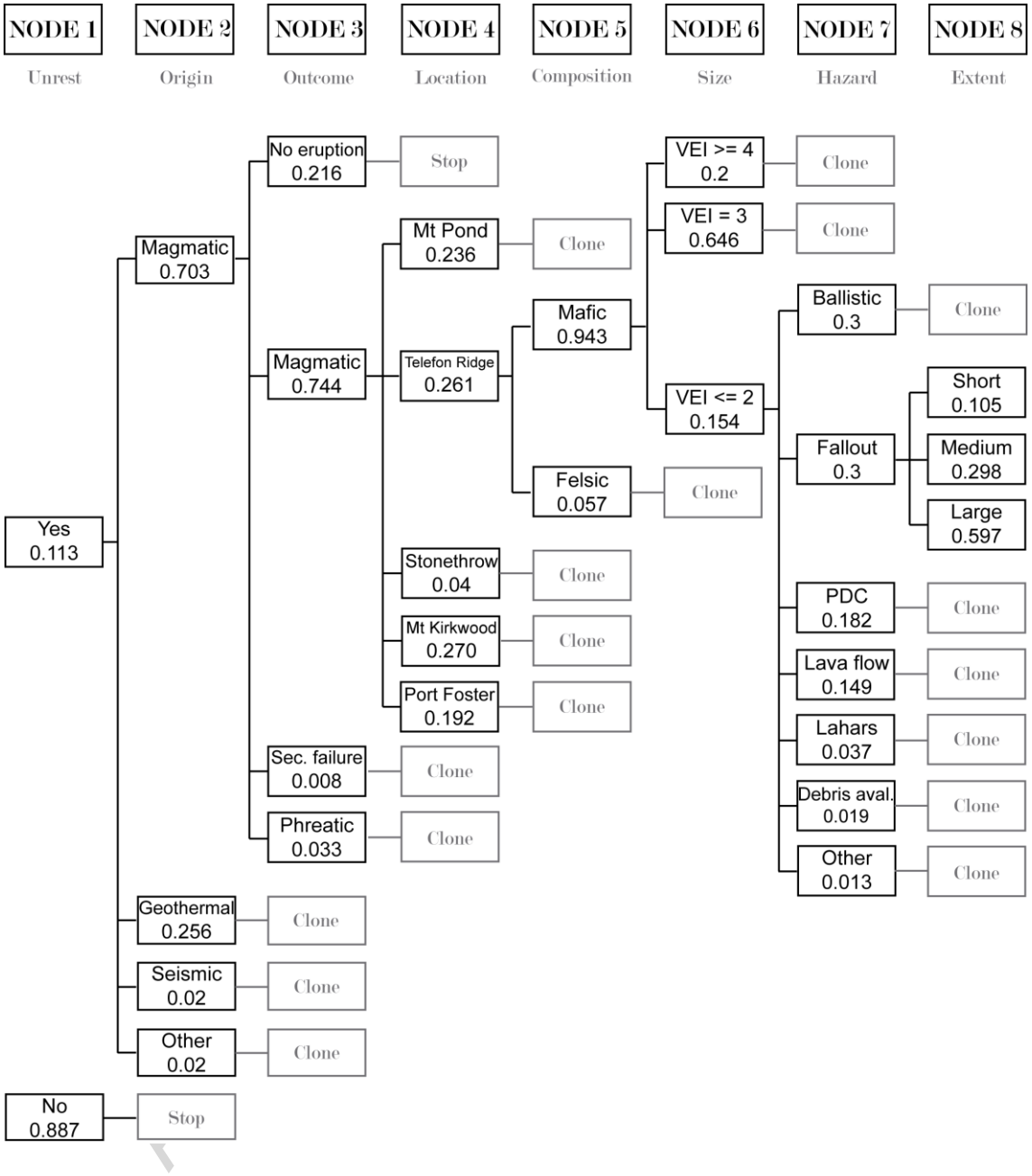

Figure 8

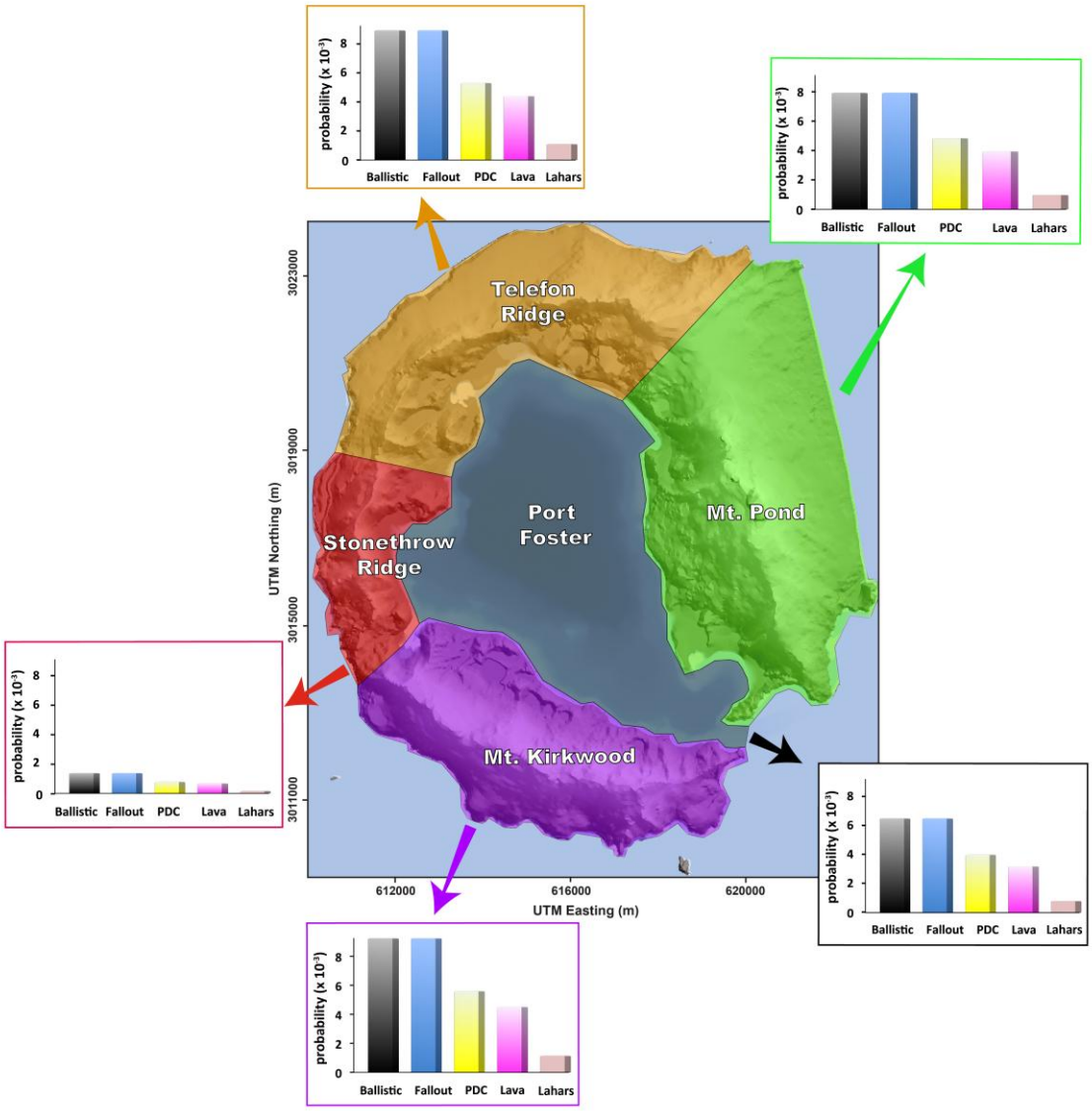

Figure 9

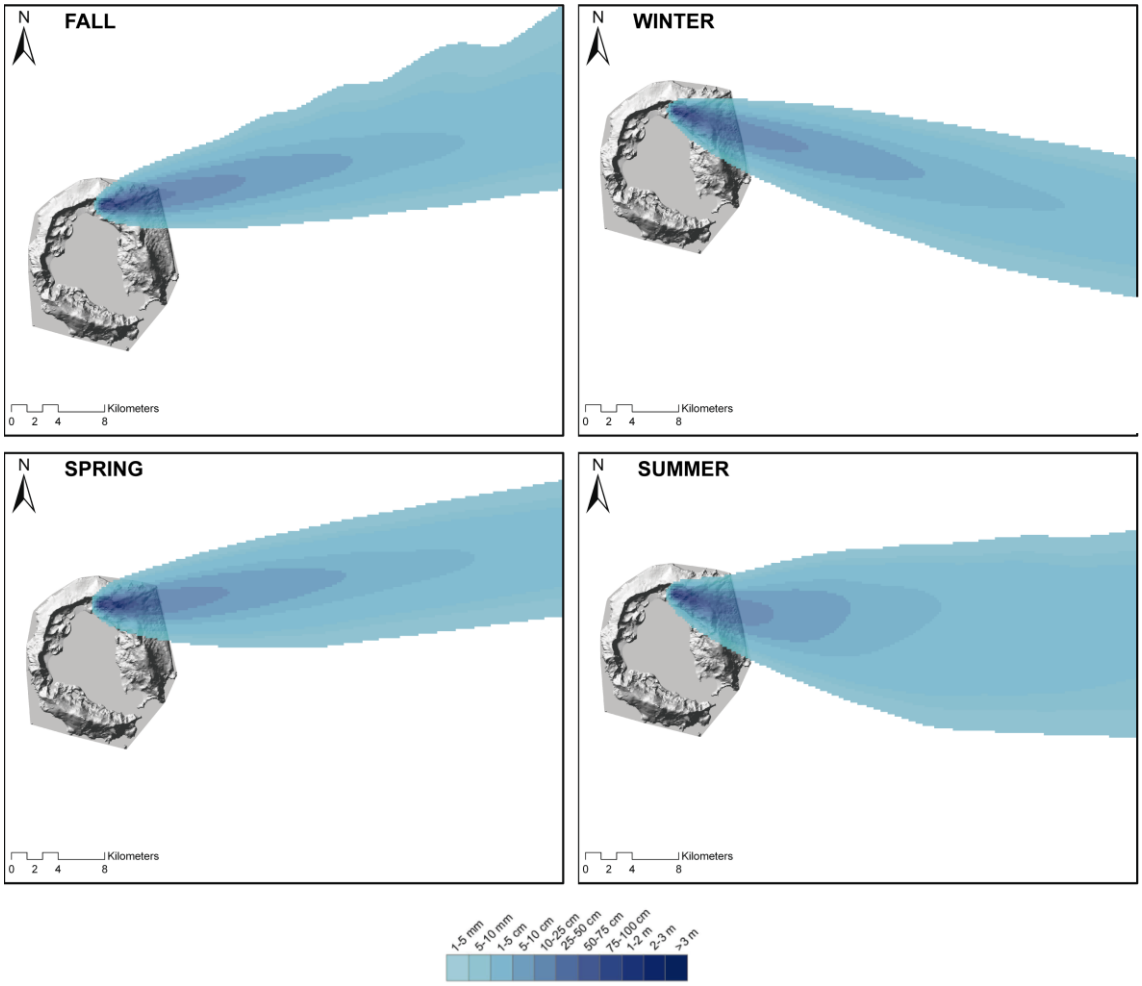

Figure 10

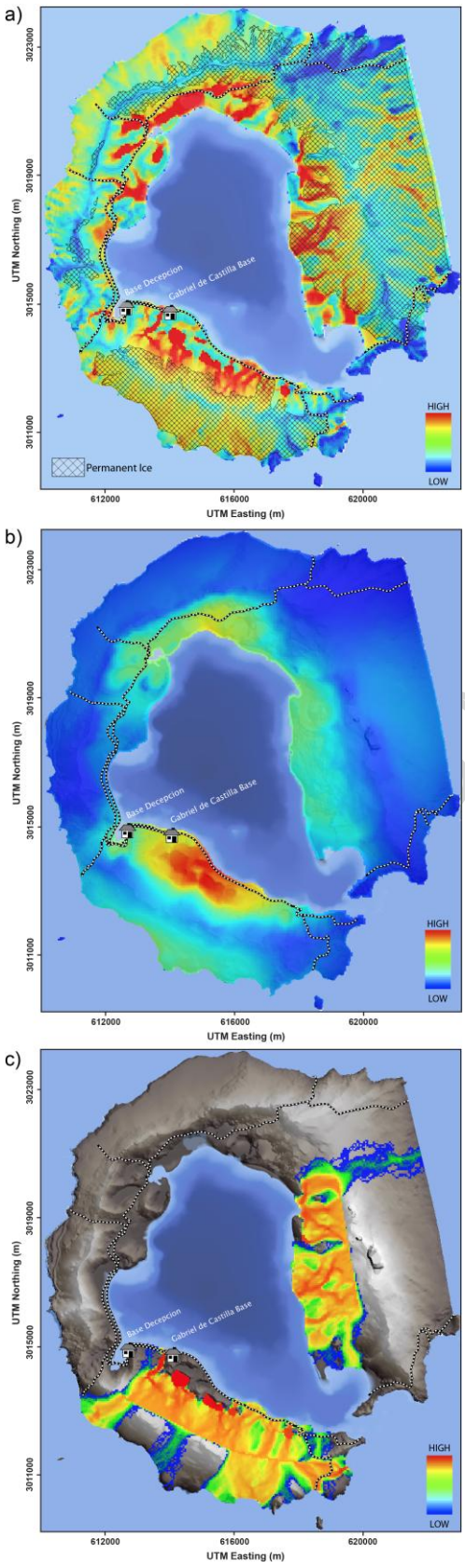

Figure 11

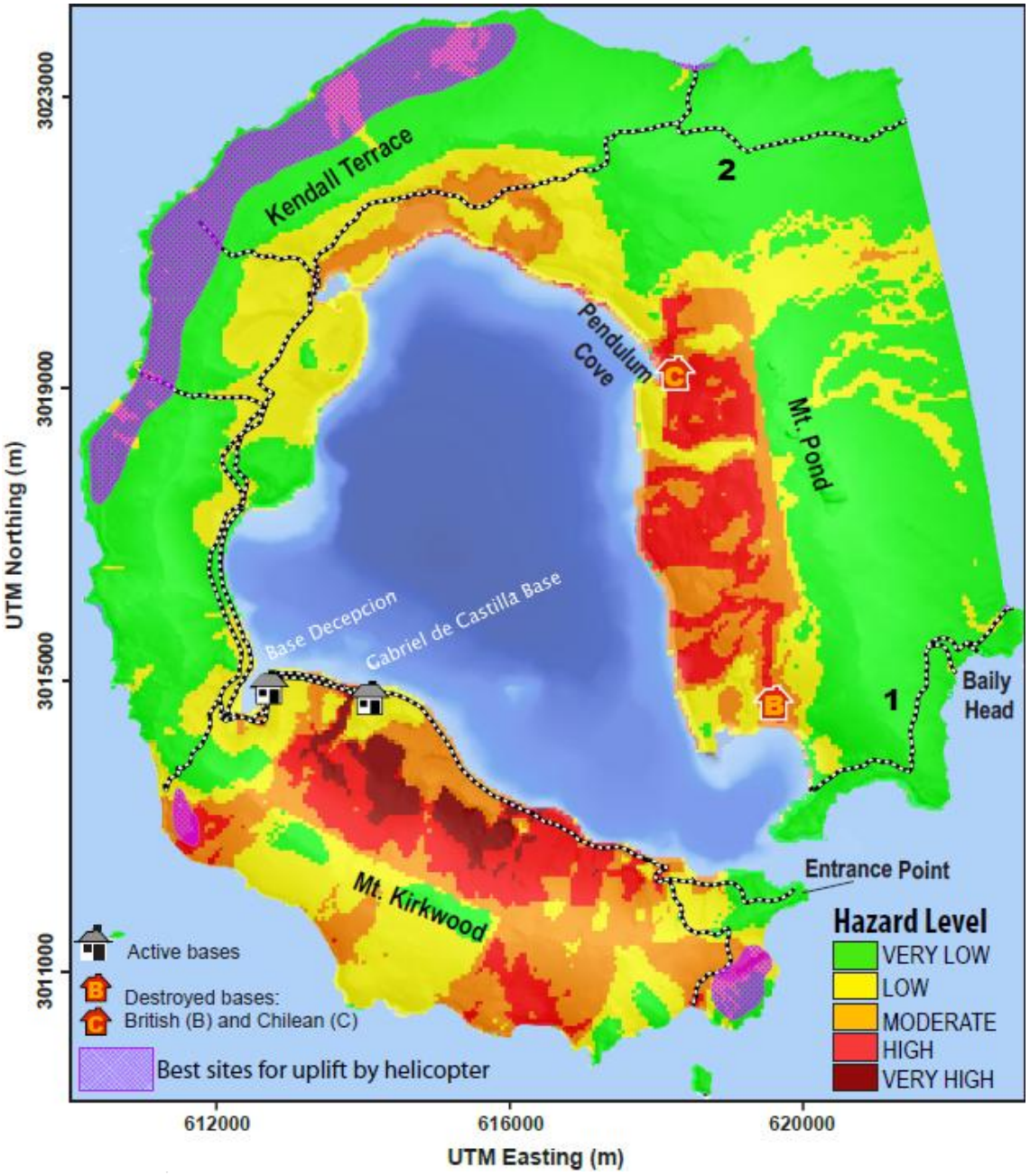

Figure 12

TABLE 1

YEAR	NODE 1	NODE 2	NODE 3	NODE 4	NODE 5	NODE 6	NODE 7	NODE 8	Source
	Unrest	Origin	Outcome	Location	Composition	Size	Hazard	Extent	
1999	Yes	Geothermal	No Eruption	-	-	-	-	-	[1]
1992	Yes	Geothermal	No Eruption	-	-	-	-	-	[1]
1970	Yes	Magmatic	Magmatic	TELEFON RIDGE	Mafic	3	Ballistic - Fall out - PDC	Large	[2] [3]
1969	Yes	Magmatic	Magmatic	MT POND	Mafic	3	Lava flow – Lahars - PDC	Medium	[3]
1967	Yes	Magmatic (?) Seismic	Magmatic	TELEFON RIDGE & PORT FOSTER	Mafic	3	Ballistic - Fall out - PDC	Medium	[3] [4]
1943± 12*	Yes	Magmatic	Magmatic	MT POND	Mafic	>=3	-	-	[5] [6]
1918 ± 12	Yes	Geothermal	No Eruption	-	-	-	-	-	[7] [8]
1915 ± 3	Yes	Magmatic	Magmatic	-	Mafic	3	Ballistic - Fall out	Large	[6] [9]
1892 ± 64	Yes	Magmatic	Magmatic	TELEFON RIDGE	-	<3	-	-	[5]
1879 ± 49	Yes	Magmatic	Magmatic	MT POND	-	<=3	Ballistic - Fall out - Lava flow	-	[10]
1869 ± 40	Yes	Magmatic	Magmatic	MT POND	Mafic	<=3	-	-	[5]
1842	Yes	Magmatic	Magmatic	MT KIRKWOOD	Felsic	2	Lava flow	Small	[7] [11] [12]
1838 - 1839	Yes	Magmatic	Magmatic	MT KIRKWOOD	-	>3	Lava flow	-	[6] [7] [13] [14]
1827 ± 2	Yes	Magmatic	Magmatic	MT POND	Mafic	4	-	-	[5] [7] [15] [16]
1820 ± 1	Yes	Magmatic	Magmatic	-	Mafic	<3	Ballistic - Fall out	Large	[17]
1795 ± 5	Yes	Magmatic	Magmatic	TELEFON RIDGE	-	-	-	-	[5] [7] [15] [16]
1750 ± 50	Yes	Magmatic	Magmatic	MT KIRKWOOD	Mafic	>=3	-	-	[6]
1700	Yes	Magmatic	Magmatic	-	-	>=3	-	-	[18] [19]
1641	Yes	Magmatic	Magmatic	-	Mafic	>3	Ballistic - Fall out	Large	[20] [21]

* Error according to the time interval provided by the bibliography

[1] Ibañez et al., 2003
[2] Gonzáles-Ferrán et al., 1971
[3] Baker et al., 1975
[4] Valenzuela et al., 1968
[5] Roobol, 1973
[6] Pallas et al., 2001
[7] Roobol, 1980
[8] Roobol, 1982
[9] Hodgson et al., 1998
[10] Smellie, 2002a
[11] Smiley in Wilkes, 1845
[12] Hawkes, 1961
[13] Whittle in Wilkes, 1845
[14] Birkenmajer, 1991
[15] Kendall, 1831
[16] Pallas et al., 2001
[17] Palais et al., 1989
[18] Moreton, 1999
[19] Smellie, 1999
[20] Aristain and Delmas, 1998
[21] Delmas et al., 1992

TABLE 2

YEAR (B.P.)	NODE 1 Unrest	NODE 2 Origin	NODE 3 Outcome	NODE 4 Location	NODE 5 Composition	NODE 6 Size	NODE 7 Hazard	NODE 8 Extent	Source
450	Yes	Magmatic	Magmatic	-	Mafic	>=3	-	Large	[1] [2] [3]
750	Yes	Magmatic	Magmatic	-	Mafic	>=3	-	Large	[1] [2] [3]
1050	Yes	Magmatic	Magmatic	-	Mafic	>=3	-	Large	[2] [3]
1350	Yes	Magmatic	Magmatic	-	Mafic	>=3	-	Large	[1] [2] [3]
1850	Yes	Magmatic	Magmatic	-	Mafic	>=3	-	Large	[2] [3]
2100	Yes	Magmatic	Magmatic	-	Mafic	>=3	-	Large	[2] [3]
2250	Yes	Magmatic	Magmatic	-	-	>=3	-	Large	[2] [3]
2500	Yes	Magmatic	Magmatic	-	Mafic	>=3	-	Large	[2] [3]
2700±50*	Yes	Magmatic	Magmatic	-	Mafic	>=3	-	Large	[1] [2] [3]
3500	Yes	Magmatic	Magmatic	-	-	>=3	-	Large	[2] [3]
4700	Yes	Magmatic	Magmatic	-	Mafic	>=3	-	Large	[1] [2] [3]
5200	Yes	Magmatic	Magmatic	-	Mafic	>=3	-	Large	[3] [4]
8700 (?)	Yes	Magmatic	Magmatic	-	Mafic	>=3	-	Large	[3] [4]
10670	Yes	Magmatic	Magmatic	-	Mafic	>3	-	Large	[2] [3]
21660	Yes	Magmatic	Magmatic	-	Mafic	>3	-	Large	[2] [3]
26400	Yes	Magmatic	Magmatic	-	Mafic	>3	-	Large	[2] [3]
35400	Yes	Magmatic	Magmatic	-	Mafic	>3	-	Large	[2] [3]

* Error according to the time interval provided by the bibliography

[1] Björck et al., 1991
[2] Moreton, 1999
[3] Smellie, 1999
[4] Mathies et al., 1990

TABLE 3

	Hazard factors			
		Score (max)	*Score (min)*	*References*
(a)	Volcano type	1	1	[1] [2] [3]
(b)	Maximum Volcano Explosivity Index (VEI)	1	1	[1] [2] [3]
(c)	Explosive activity	1	1	[1] [2] [3]
(d)	Major explosive activity	1	0	[1] [2] [3]
(e)	Eruption recurrence	4	4	[3] [4] [5]
(f)	Holocene pyroclastic flows?	1	1	[3]
(g)	Holocene lava flows?	1	1	[3] [4]
(h)	Holocene-lahars?	1	1	[3]
(i)	Holocene tsunami (s)?	1	1	[3]
(j)	Hydrothermal explosion potential	1	1	[3]
(k)	Sector collapse potential	1	1	[3]
(l)	Primary lahar source	1	1	[3] [4] [6]
(m)	Observed seismic unrest	1	1	[7]
(n)	Observed ground deformation	1	1	[8]
(o)	Observed fumarolic or magmatic degassing	1	1	[7]
	TOTAL HAZARD FACTORS (THF)	**18**	**16**	
	Exposure factors			
		Score (max)	*Score (min)*	*References*
(p)	Volcano Population Index (VPI) at 30 km	3	1.7	
(q)	Population downstream or downslope	0	0	
(r)	Historical fatalities	0	0	[3]
(s)	Historical evacuations	0	0	[7] [9]
(t)	Local aviation exposure	1	1	
(u)	Regional aviation exposure	2	0	
(v)	Power infrastructure	1	1	
(w)	Transportation infrastructure	1	1	
(x)	Major development or sensitive areas	1	1	
(y)	Volcano is a significant part of a populated island	1	1	
	TOTAL EXPOSURE FACTORS (TEF)	**10**	**6.7**	
	Relative Threat Ranking (*THF ×TEF)*	**180**	**107.5**	

[1] Aristain and Delmas, 1998
[2] Caselli and Agusto, 2004
[3] Smellie, 2002a
[4] Roobol, 1982
[5] Orheim, 1972
[6] Baker et al., 1975
[7] Ibañez et al., 2003
[8] Prates et al., 2013
[9] Smith et al., 2003

TABLE 4

BANDWIDTH PARAMETER	
LAYER	*h* (m)
Post-caldera craters (field work, analyzing orthophotos)	1170
Historic volcanism (Wilkes, 1845; Valenzuela et al., 1970; González-Ferrán et al., 1971; Baker et al., 1975; Roobol, 1980; Smellie, 2002b; Pedrazzi et al., 2014)	528
Lineaments (Martí et al., 2013)	3294
Fumarolic activity (Lòpez-Martinez et al., 2000; Smellie and Lòpez-Martinez, 2002)	4071
Heated ground (Lòpez-Martinez et al., 2000; Smellie and Lòpez-Martinez, 2002)	1001

TABLE 5

	NODE NAME	EVENT	PAST DATA	PRIOR WEIGHT	DATA WEIGHT
1	UNREST	Yes	19	0.30	10
1	UNREST	No	167	0.70	10
2	ORIGIN	Magmatic	16	0.50	10
2	ORIGIN	Geothermal	3	0.40	10
2	ORIGIN	Seismic	0	0.05	10
2	ORIGIN	Other	0	0.05	10
3	OUTCOME	Magmatic eruption	16	0.6	10
3	OUTCOME	Sector Failure	0	0.02	10
3	OUTCOME	Phreatic eruption	0	0.08	10
3	OUTCOME	No eruption	3	0.30	10
4	LOCATION	Mt. Pond	5	0.20	50
4	LOCATION	Telefon Ridge	4	0.25	50
4	LOCATION	Stonethrow Ridge	0	0.05	50
4	LOCATION	Mt. Kirkwood	3	0.28	50
4	LOCATION	Port Foster	1	0.22	50
5	COMPOSITION	Mafic	10	0.95	50
5	COMPOSITION	Felsic	1	0.05	50
6	SIZE	VEI >= 4	3	0.20	10
6	SIZE	VEI = 3	9	0.70	10
6	SIZE	VEI <= 2	3	0.10	10
6	SIZE	-	-	-	-
7	HAZARD	Ballistic	6	0.30	30
7	HAZARD	Fallout	6	0.30	30
7	HAZARD	PDC	3	0.20	30
7	HAZARD	Lava flow	4	0.12	30
7	HAZARD	Lahars	1	0.03	30
7	HAZARD	Debris avalanche	0	0.03	30
7	HAZARD	Other	0	0.02	30
8	EXTENT	Short	1	0.10	50
8	EXTENT	Medium	2	0.30	50
8	EXTENT	Large	4	0.60	50

Highlights

- We present the long-term volcanic hazard assessment on Deception Island
- We use an statistical method to calculate eruption recurrence (HASSET)
- We estimate the probability of new vent opening based on geologicalrecord
- We evaluate the potential extent of the main expected volcanic hazards
- Results obtained are potentially useful for long-term emergency planning